UNIVERSITÀ
DEGLI STUDI
DI BRESCIA

DOTTORATO DI RICERCA IN TECHNOLOGY FOR HEALTH

Settore scientifico disciplinare: MED/04

CICLO: XXXIV

BUILDING ENGINEERED HUMAN TISSUES: FROM CELL AGGREGATES TO ORGANOIDS

RELATORE

Dott.ssa Patrizia Dell'Era, Università degli Studi di Brescia

DOTTORANDA

Dott.ssa Marialaura Serzanti

Contents

ABSTRACT

L'inaccessibilità in vivo ad alcuni tipi di campioni umani e le differenze tra modelli animali e fisiologia umana ostacolano lo studio dell'organogenesi e della patogenesi di importanti malattie umane. Una comprensione più approfondita delle tecniche di coltura cellulare tridimensionale (3D) e dei protocolli di differenziazione ha consentito l'istituzione di sistemi di coltura di organoidi (ORG). Gli ORG epatici possono essere utilizzati per il disease modeling e lo screening dei farmaci, nonché per studiare lo sviluppo del fegato. Gli ORG sono una tecnologia potente in molte applicazioni biologiche e cliniche, grazie alla loro architettura 3D fisiologica e alla loro ampia versatilità in termini di tipi di tessuto ottenibili; gli ORG, infatti, sono stati utilizzati in numerosi studi biomedici su modelli di malattie, medicina di precisione e studi tossicologici. Gli ORG epatici derivati dai pazienti possono essere uno strumento cruciale per studiare i meccanismi di malattie, come le condizioni genetiche ereditarie e il cancro. Quando si passa da una coltura cellulare 2D a un costrutto 3D, è importante considerare il mantenimento del trasporto di massa. La sopravvivenza cellulare, infatti, dipende non solo dalla capacità di fornire nutrienti e ossigeno, ma anche dalla rimozione dei prodotti di scarto e dei metaboliti.

Sebbene l'approccio basato su ORG rimanga molto promettente, l'uso degli ORG epatici su larga scala deve superare le attuali sfide tecnologiche e biologiche inerenti al controllo della composizione in cellule, delle dimensioni, e della forma degli ORG. I numerosi progressi compiuti nel set up di condizioni di coltura 3D, in grado di monitorare e controllare specifici fattori ambientali attraverso l'uso di bioreattori, forniscono tecnologie nuove e migliori per soddisfare i requisiti di riproducibilità. In questa prospettiva, il nostro lavoro ha avuto come scopo lo sviluppo di ORG epatici umani come modello 3D affidabile per il disease modeling e lo screening di farmaci. Il nostro obiettivo principale era impostare e ottimizzare i protocolli utilizzati per ottenere gli ORG in modo riproducibile per poi caratterizzarli. Abbiamo utilizzato particolari piastre appositamente progettate per ottenere microaggregati cellulari 3D. Non solo l'utilizzo di queste piastre ha garantito un accettabile grado di variabilità in termini di dimensione degli aggregati, ma l'ele-

vato numero di micropozzetti su ciascuna piastra ha permesso facilmente la produzione di un grande numero di sferoidi/organoidi. Inoltre, abbiamo coltivato gli ORG in condizioni di coltura 3D dinamiche e statiche; studiandone gli effetti sulle cellule e identificando la condizione di coltura con i migliori risultati in termini di vitalità e comportamento cellulare. Per farlo abbiamo utilizzato un bioreattore a perfusione: il LiveBox1 di IVTech; un piccolo bioreattore, paragonabile nelle dimensioni ai classici strumenti di coltura come piastre di Petri, che consente l'uso di un numero inferiore di cellule e volumi di terreno di coltura inferiori, rispetto ad altri bioreattori, un punto cruciale quando si lavora con cellule differenziate da cellule staminali pluripotenti indotte (iPSC). Nel nostro studio preliminare, abbiamo dimostrato che l'utilizzo di una condizione di coltura dinamica, come il bioreattore LiveBox1, ha aumentato la vitalità degli organoidi in esso coltivati. Utilizzando una linea iPSC di controllo abbiamo differenziato e caratterizzato cellule staminali mesenchimali indotte (iMSC) ed epatociti indotti (iHEP) da utilizzare per assemblare gli organoidi. Entrambi i tipi cellulari ottenuti esprimono marcatori e proprietà caratteristici, confermando così la loro natura. In conclusione, sebbene la creazione e l'ottimizzazione di un modello di organoide 3D possano essere impegnative, i vantaggi e le possibilità che questo strumento ha da offrire superano gli sforzi necessari.

LIST OF ABBREVIATIONS

2D	two-dimensional
3D	three dimensional
AAT	Alpha-1 Antitrypsin
Act A	Activin A
AF	anterior foregut
AFP	Alpha Fetoprotein
ALB	albumin
ALT	Alanine Transaminase
AP	Alkaline Phosphatase
ASCs	Adult Stem Cells
AST	Aspartate Transaminase
bFGF/FGF2	basic Fibroblast Growth Factor
BMP	Bone Morphogenetic Proteins
BSA	bovine serum albumin
CF	cystic fibrosis
CFTR	cystic fibrosis transmembrane conductance regulator
DAB	diaminobenzydine
DE	definitive endoderm
DMEM	Dulbecco's modified Eagle's medium
EBs	embryoid bodies
ECM	Extra-Cellular Matrix
EGF	epidermal growth factor
EHS	Engelbreth-Holm-Swarm
ESCs	Embryonic Stem Cells
FBS	fetal bovine serum
Fc	centrifugal force
Fd	drag force
Fg	gravitational force
FGF	Fibroblast Growth Factor
FSK	forskolin
GI	gastrointestinal
Hep G2	Human hepatoma cells
HFF	Human Foreskin Fibroblasts
HGF	Hepatocyte Growth Factor
HUVECs	Human umbilical vein endothelial cells
ICM	inner cell mass
iHEPs	Human-induced Hepatocytes
iMSCs	induced Mesenchymal Stem Cells

iPSCs	Induced Pluripotent Stem Cells
ISCT	International Society for Cellular Therapy
LB1	LiveBox1
MC	mixed cell population
MLD	Monogenic liver diseases
mMC	mock mixed culture
mORG	mock organoids
MSCs	mesenchymal stem cells
ORGs	organoids
OSM	Oncostatin M
PF	posterior foregut
PLC	primary liver cancer
PSCs	pluripotent stem cells
RWV	rotating-wall vessel
SPHs	spheroids
TBS	tris-buffered saline
TGFbi	transforming growth factor beta inhibitor
TNFa	tumour necrosis factor-alpha

INTRODUCTION

ORGANOIDS

The inaccessibility to some types of human samples *in vivo* and the differences between animal models and human physiology hamper the study of human organ development and the pathogenesis of important human diseases. Deeper understanding in three dimensional (3D) cell culture techniques and differentiation protocols have allowed the institution of organoid (ORG) culture systems. Lancaster and Knoblich define ORGs as "containing several cell types that develop from stem cells or organ progenitors and self-organize through cell sorting and spatially restricted lineage commitment, similar to the process *in vivo*."(1)
In order to be considered as such, ORGs must resemble the actual organ in terms of being composed of more than one cell type of the *in vivo* organ; they should have some specific function of that organ; and the cellular organization should be similar to that of the organ itself (1). The complex microenvironments in which cells naturally reside provide stimuli such as signaling interactions from soluble factors, mechanical interactions and the Extra-Cellular Matrix (ECM). These stimuli are crucial for maintaining and regulating the cells' functions and phenotypes. From literature, we now know that cells cultured in 3D, in conditions similar to their native ones, more closely resemble their *in vivo* counterparts as compared with cells cultured in classical two-dimensional (2D) techniques (2).

In the early 1960s, a number of studies were conducted to comprehend the tissue patterning process (Fig. 1); mainly using dissociation and reaggregation of tissues to understand the movements of cells *in vitro*. Weiss and Taylor, among others, (3) demonstrated that by taking chick embryo's dissociated kidney cells and putting them back together, they could obtain aggregates that recapitulate renal development. This and other studies confirm that organs can self-assemble, due to two main processes:

- cells with similar adhesive properties segregate into thermodynamically stable domains (4);

- spatially determined fate decision (5) (Fig. 2).

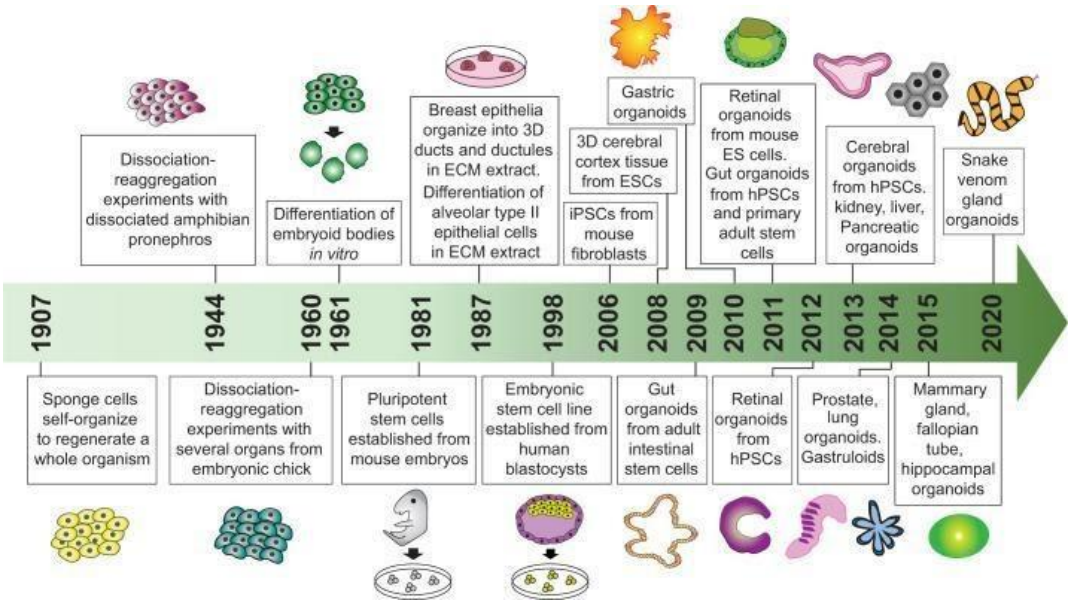

Figure 1. Timeline for the development of organoid cultures. A summary of key landmark studies and breakthroughs leading to the establishment of various organoid technologies. 3D, 3-dimensional; ECM, extracellular matrix; ESCs, embryonic stem (ES) cells; hPSCs, induced pluripotent stem cells (Corrò et al., 2020).

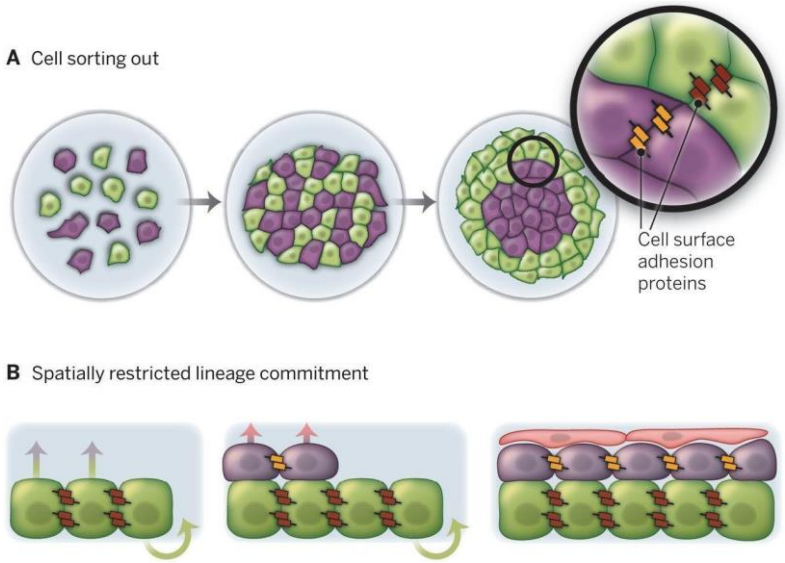

Figure 2. (A) Cell sorting out describes the movement of cells into different domains. Different cell types (purple or green) sort themselves because of different adhesive properties conferred by their differential expression of distinct cell adhesion molecules (shown as brown or orange bars). (B) Spatially restricted cell-fate decisions also contribute to self-organization in vivo and in organoids. Progenitors (green) give rise to more differentiated progeny (purple), which, because of spatial constraints of the tissue and/or division orientation, are forced into a more superficial position that promotes their differentiation. These cells can sometimes further divide to give rise to more differentiated progeny (pink), which are further displaced (Lancaster et al., 2014).

These two mechanisms are particularly evident in the formation of teratomas, tumors that originate from pluripotent stem cells (PSCs). These tumors are com-

posed by different organized tissues, spontaneously developed presumably from a combination of both cell segregation and fate determination; both requiring the activation of numerous signaling pathways mediated by cellular components or environmental factors such as ECM and cell culture medium.

Different cell types can be used to derive ORGs:

- Embryonic Stem Cells (ESCs);
- Induced Pluripotent Stem Cells (iPSCs);
- Neonatal or Adult Stem Cells (ASCs) (6, 1) (Fig. 3).

When deriving ORGs from ESCs or iPSCs, differentiation steps are required, involving protocols based on the time-related use of growth factors or inhibitors resembling the developmental cues specific to organogenesis. The pluripotent capacity of iPSCs not only allows the generation of ORGs from the three germ layers, but also the generation of patient-specific ORGs, for disease modeling and drug screening.

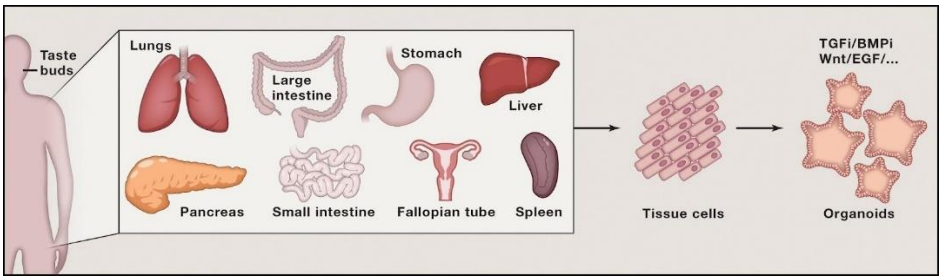

Figure 3. Schematic of the various regions of the body that can be cultured as aSC-Derived (Clevers et al., 2016)

Since this process depends on spatial organization, it is crucial to have a 3D microenvironment to give the cells the opportunity to self-assemble *in vitro*; this may be achieved using either scaffold or scaffold-free techniques.

For a scaffold-free technique, cells can be cultured in hanging drops, relying on surface tension and gravity.

Alternatively, scaffolds can be composed by either biological or synthetic gels that mimic the natural ECM specific to the tissue in study in which the cells will be embedded. The most commonly used ECM is Matrigel, a protein mixture secreted by Engelbreth-Holm-Swarm (EHS) mouse sarcoma cells (7); this matrix gives crucial structural support as well as ECM molecular and mechanical signals to the cells.

LIVER ORGANOIDS

The zygote is a single totipotent cell which proliferates and forms cells that become more and more lineage-restricted. When the blastocyst stage is reached, the outer cells are committed to become extraembryonic tissues, while the cells of the inner cell mass (ICM) are pluripotent and give rise to all the embryo's tissues. During the gastrulation process, the cells derived from the ICM form the three germ layers: endoderm, mesoderm, and ectoderm. Within each germ layer, progenitor cells specify to form embryonic organ structures, from which all tissues and organs will develop (Fig. 4).

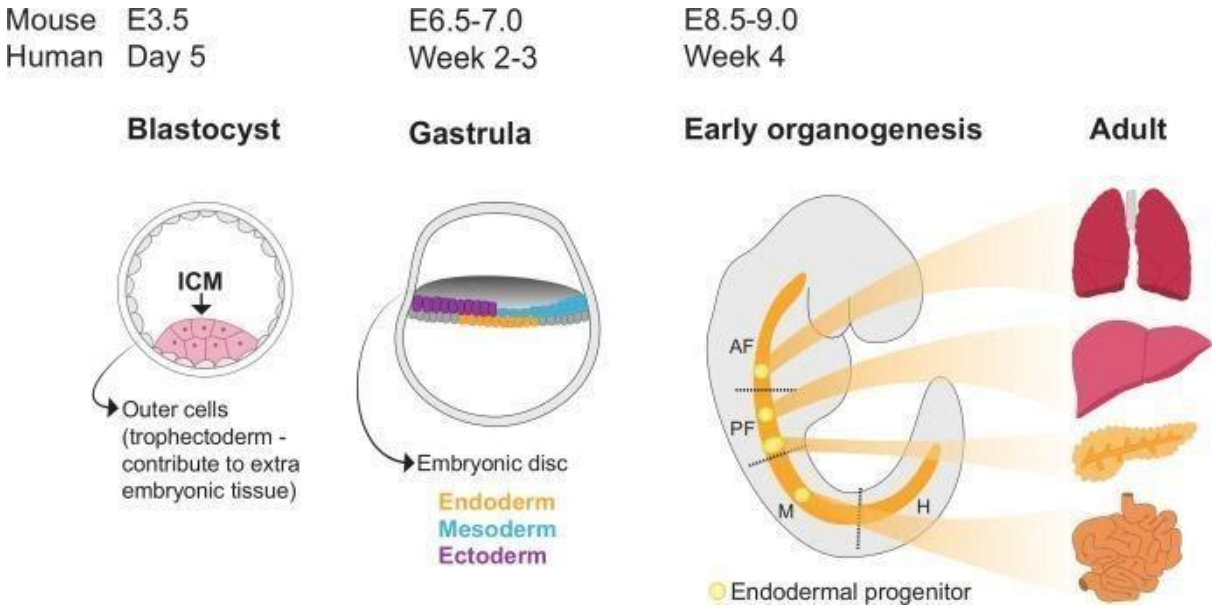

Figure 4. Organogenesis and stages for organoid progenitor isolation. Schematic depicting key stages of organogenesis timings in mice and humans. Following fertilization and cleavage of the embryo, the blastocyst is formed in which cells segregate into the outer layer and the inner cell mass (ICM). Cells of the ICM are pluripotent and can be isolated to generate embryonic stem cells. The next key developmental milestone is gastrulation, a process whereby cells derived from the ICM undergo dynamic cell movements and rearrange to form the three germ layers: endoderm, mesoderm and ectoderm. Here we depict a human gastrula which develops as an embryonic disc (note: gastrulation in mice occurs as an egg cylinder). As development progresses, progenitors within each germ layer become specified to give rise to specific tissues and organs. The identities of the progenitors are influenced by their anterior-posterior and dorsal-ventral positions in the embryo. The endoderm becomes patterned along the anterior-posterior axis into the anterior foregut (AF), posterior foregut (PF), midgut (M) and hindgut (H). Illustrated here are a selection of organs that derive from the different endodermal domains: AF—lungs; PF—liver and pancreas; M—small intestine. The hindgut gives rise to more posterior tissues such as the colon. Organoids can be derived from tissue-resident progenitors isolated at both organogenesis stages and from adult tissues (Prior et al, 2019).

From the endoderm, a tube forms the gastrointestinal (GI) tract, in which three different portions can be identified: the foregut, the midgut, and the hindgut (8).

From the foregut originate the oral cavity, pharynx, respiratory tract, pancreas, stomach, and the liver; the small intestine and the ascending colon come from the midgut, and from the hindgut develop the remaining colon and the rectum.
The foregut endoderm epithelium gives rise to the liver by originating the hepatic bud structure, from which hepatoblasts generate (9).
Hepatoblasts undergo cell shape changes, in response to signaling factors such as Fibroblast Growth Factor (FGF), Bone Morphogenetic Proteins (BMP), Hepatocyte Growth Factor (HGF) and Wnt, secreted by the surrounding microenvironment; along with cell shape changes, the cells proliferate and migrate, becoming lineage-committed and giving rise to hepatocytes and cholangiocytes (10).
The hepatocytes and cholangiocytes composing the liver work together with stromal, endothelial, and mesenchymal cells to perform their physiological role, maintaining the body homeostasis through metabolic, exocrine and endocrine functions (11).

Many studies obtained liver ORGs using different methods and different cell sources (Fig. 5).
Weiss *et al.* demonstrated that, after dissociation, chick embryonic hepatic tissue can reaggregate and form secretory units with functional bile ducts (3). Huch *et al.* collected Lgr5+ hepatic cells from mice, seeded them in 3D with Matrigel and obtained ORGs from which mature, functional hepatocytes could be differentiated (12). In a follow up study, bipotent progenitors derived from adult bile ducts were established from human liver (13). Takebe *et al.* described a protocol involving iPSCs to generate vascularized human liver: human iPSCs were differentiated into hepatic endodermal cells in 2D and assembled together with human mesenchymal stem cells (MSCs) and human endothelial cells in spontaneously forming 3D aggregates (14).
Liver ORGs can be used for disease modeling and drug screening, as well as studying liver development.

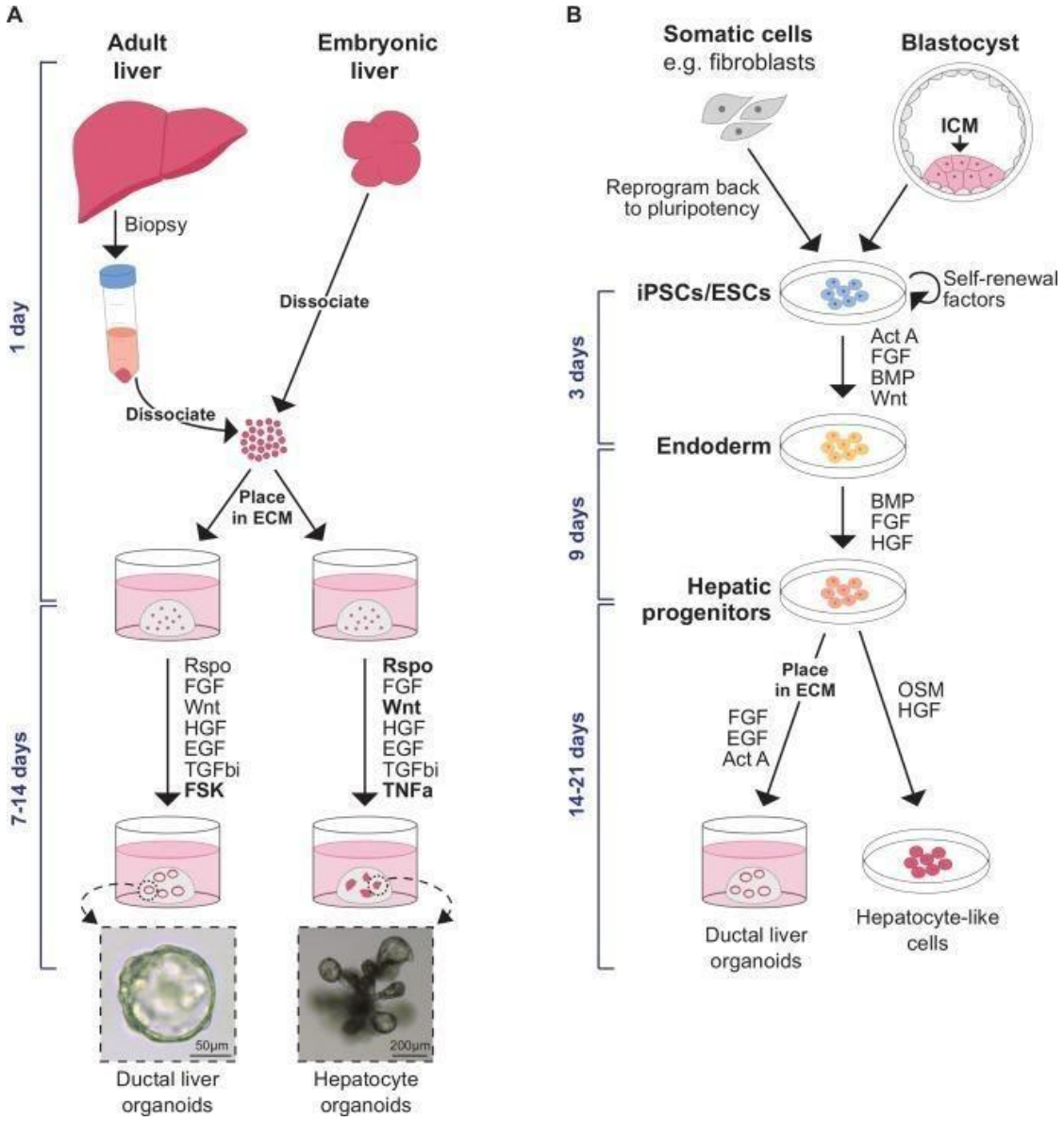

Figure 5. Liver organoids can be derived from various cells of origin by regulating signaling pathways during in vitro culture. (A) Liver organoids can be formed from tissue-resident cells isolated from biopsies of adult tissues or from embryonic stages during organogenesis. Hepatoblasts (the bipotent embryonic progenitors in vivo which give rise to ductal cells and hepatocytes) can be placed in Matrigel as ECM and generate ductal or hepatocyte organoids depending on the growth factors supplemented in the culture medium. (Bright-field images of mouse embryonic ductal and hepatocyte organoids taken from Prior et al., 2019). Signalling pathways which are typically modulated to enable organoid formation are listed; the pathways which are essential for different types of liver organoids are in bold. Formation of ductal or hepatocyte organoids from adult tissues requires the isolation of appropriate cells of origin. In order to generate ductal hepatic organoids from adult tissues, ductal fragments or ductal cells can be placed in Matrigel with the optimized media. Formation of adult hepatocyte organoids requires the isolation of mature hepatocytes. (B) Liver organoids can also be generated from pluripotent stem cells (iPSCs and ESCs), usually by a three-stage differentiation process that recapitulates the signaling programs active during development. iPSCs/ESCs are first directed towards an endodermal fate by exposure to Act A and Wnt. These endoderm cells then progress to a hepatic fate following induction of HGF and FGF signaling. These hepatic progenitors are hepatoblast-like cells. The hepatic progenitors can form hepatocyte-like cells in response to OSM signaling. Conversely, by placing the hepatic progenitors in ECM and modulating FGF, EGF and Act A signaling, ductal organoids can be generated. Act A, Activin A; BMP, bone morphogenetic protein; ECM, extracellular matrix; EGF, epidermal growth factor; ESCs, embryonic stem cells; FGF, fibroblast growth factor; FSK, forskolin; HGF, hepatocyte growth factor; ICM, inner cell mass; iPSCs, induced pluripotent stem cells; OSM, Oncostatin M; TGFbi, transforming growth factor beta inhibitor; TNFa, tumour necrosis factor-alpha (Prior et al., 2019).

LIVER ORGANOIDS FOR DISEASE MODELING

ORGs are a powerful technology in many biological and clinical applications (Fig. 6), due to their physiological 3D architecture and their wide versatility in terms of obtainable tissue types; ORGs, in facts, have been used in a high number of biomedical studies for disease modeling, precision medicine, and toxicology studies (21).

Patient-derived liver ORGs can be a crucial tool to investigate the mechanisms of diseases, such as hereditary conditions and cancer.

Monogenic liver diseases (MLD) are caused by single gene mutations and are classified in three groups based on the extent of the parenchyma damage and/or specific liver expression:

- conditions characterized by liver parenchymal damage and hepatic injury,
- disorders in which the liver is structurally normal,
- diseases characterized by systemic and hepatic clinical manifestations. (15)

Alpha-1-anti-trypsin (AAT) deficiency is an example of a monogenic disorder affecting the liver parenchyma (15). Tissue from patients with AAT deficiency was used to derive ORGs; as observed in the original biopsy, these liver ORGs accumulate protein aggregates (12).

Genetic disorders from the second group are defects in which extrahepatic complications are the main cause of death, while the liver architecture and function are generally preserved (15).

Within the third group of monogenic diseases, cystic fibrosis (CF) was the first monogenic disease modelled with ORGs (11). CF is caused by a plethora of mutations in the cystic fibrosis transmembrane conductance regulator (CFTR) chloride channel, normally expressed in epithelial cells of different organs (16). Dekkers and colleagues (17) obtained human intestinal ORGs from rectal biopsies of CF patients and showed that these ORGs recapitulated the disease *in vitro* when cultured with an activator. Sampaziotis and colleagues (18) and Ogawa and colleagues (19) generated cholangiocyte ORGs from iPSCs derived from CF patients and demonstrated that these ORGs could also be used to model CF *in vitro*.

These and other studies confirm that the liver ORG model recapitulates *in vitro* the key aspects of the disease in exam and allows a better understanding of the pathological processes.
Moreover, ORGs not only can be used to model genetic pathologies, but also to model acquired liver diseases such as primary liver cancer (PLC) and hepatitis. ORGs are a very useful tool in cancer studies: they allow to take in consideration the complex histoarchitecture of the tumorous mass. Studies have shown that tumor ORGs - tumouroids - maintain tissue of origin features over time (11), thus enabling the identification of genes potentially important in human liver cancer development.

DRUG SCREENING FOR LIVER TOXICITY

The primary reason for drug removal from the market is acute liver failure (20) and many clinical trials fail because of an inadequate evaluation of the drug toxicity at the preclinical stage (21); this happens because animal models often metabolize drugs in a different way from the human liver, having its distinct metabolism (1).
In this view, an emerging application for liver ORGs is the establishment of biobanks containing both pathogenic and healthy liver cells to be used as screening platforms to identify drug efficacy against, potentially, any liver disease, or predict drug-induced liver injury (11).

3D CULTURE

Traditionally, the substrates mainly used for cell culture have been 2D polystyrene or glass surfaces (22). The major issue about this technique is the assumption that a cellular monolayer can accurately reproduce animal physiology: native tissues are clearly different from a 2D layer in terms of morphology, ECM, and spatial organization; resulting in differences in receptor expression, transcriptional expression, cellular migration, and apoptosis when compared to the 2D *in vitro* model (23).

To overcome these problems, many 3D methods taking into account the cell's spatial organization have been developed.

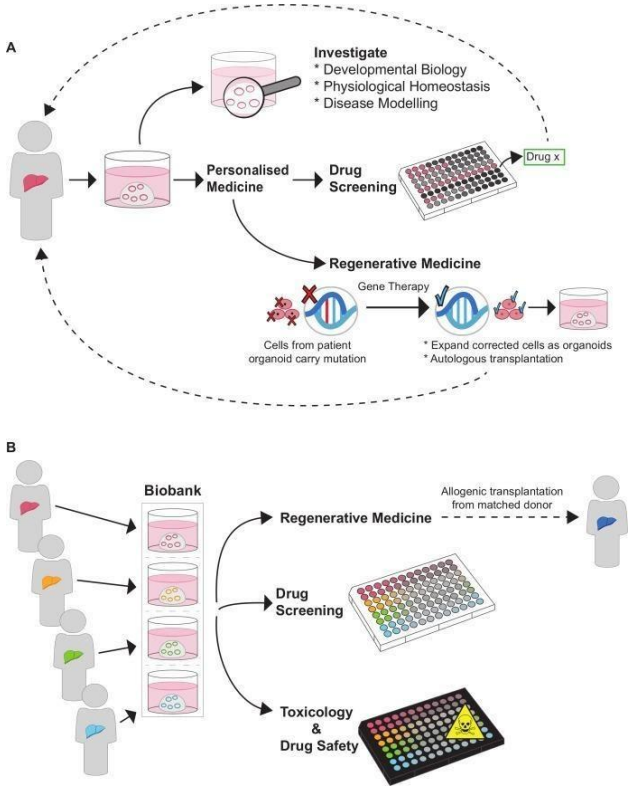

Figure 6. Applications of liver organoids. (A) Organoids derived from healthy donors or patients can be used as a model in basic research to investigate liver development and function in healthy conditions and to dissect the mechanisms of disease. Liver organoids are also a potential bridging tool towards personalised medicine, allowing for patient-specific drug screening and gene therapy. (B) Organoids can be expanded in vitro and cryopreserved enabling the establishment of biobanks. These can be used on a larger scale for regenerative medicine (including transplants), drug screening (patient-derived organoids can help identify drugs that a cohort of patients are most likely to respond to) and toxicology studies for predicting which potential therapies may induce drug-induced liver injury (Prior et al., 2019).

When switching from a 2D cell culture to a 3D construct, it is important to consider the maintenance of mass transport (24, 25). In fact, cell survival depends not only on the ability to supply nutrients and oxygen, but also on the removal of waste products and metabolites. Studies have shown that spheroids with diameters greater than 1 mm present a hypoxic core with necrotic cells, surrounded by an outer layer of living cells (26, 27); hence why, this is a crucial consideration in the development of 3D culture systems.

DYNAMIC 3D CULTURE

In early studies, 3D culture models relied on static methods, whereas nowadays the use of bioreactors is more and more common. Bioreactors allow the control in a precise and reproducible way of environmental conditions required for cell culture, such as temperature, pH, flow rate, oxygen, nutrient supply, and waste metabolite removal.

One of the most basic bioreactors is represented by a stirred flask (Fig. 7a), in which oxygen and nutrients are mixed. However, the turbulent eddies generated in this kind of bioreactor could have negative effects on cells sensitive to mechanical stimuli (28).

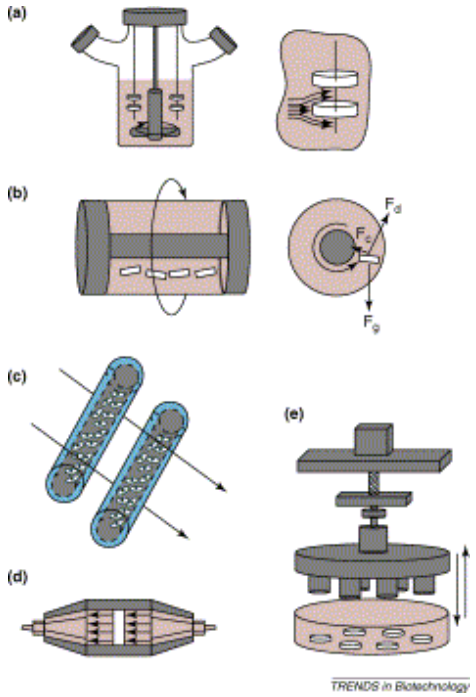

Figure 7. Representative bioreactors for tissue engineering applications. (a) Spinner-flask bioreactors have been used for the seeding of cells into 3D scaffolds and for subsequent culture of the constructs. During seeding, cells are transported to and into the scaffold by convection. During culture, medium stirring enhances external mass-transfer but also generates turbulent eddies, which could be detrimental for the development of the tissue. (b) Rotating-wall vessels provide a dynamic culture environment to the constructs, with low shear stresses and high mass-transfer rates. The vessel walls are rotated at a rate that enables the drag force (Fd), centrifugal force (Fc) and net gravitational force (Fg) on the construct to be balanced; the construct thus remains in a state of free-fall through the culture medium. (c) Hollow-fiber bioreactors can be used to enhance mass transfer during the culture of highly metabolic and sensitive cell types such as hepatocytes. In one configuration, cells are embedded within a gel inside the lumen of permeable hollow fibers and medium is perfused over the exterior surface of the fibers. (d) Direct perfusion bioreactors in which medium flows directly through the pores of the scaffold can be used for seeding and/or culturing 3D constructs. During seeding, cells are transported directly into the scaffold pores, yielding a highly uniform cell distribution. During culture, medium flowing through the construct enhances mass transfer not only at the periphery but also within its internal pores. (e) Bioreactors that apply controlled mechanical forces, such as dynamic compression, to engineered constructs can be used as model systems of tissue development under physiological loading conditions, and to generate functional tissue grafts. Compressive deformation can be applied by a computer-controlled micro-stepper motor, and the stress on the constructs can be measured using a load cell (Martin et al., 2004)

In order to generate low shear forces, an efficient alternative consists in using a rotating fluid environment, producing a dynamic laminar flow. Many different cell types have been used in rotating-wall vessel (RWV) bioreactors (Fig. 7b) for tissue generation included but not limited to chondrocytes (26), cardiac cells (29) and various tumor cells (30, 31). These studies show that the morphological, biochemical and physiological properties of the cells grown in the RWV bioreactors resembled their *in vivo* counterparts more closely than the static or stirred-flasks cultured ones.

Another type of bioreactors are the direct perfusion ones (Fig. 7d). These bioreactors increase the mass transport of nutrients and oxygen by perfusing culture medium either through or around semi-permeable fibers or directly through the pores of cell-seeded 3D scaffolds. It is very important to optimize the bioreactor's medium flow-rate, to balance the mass transfer of nutrients and waste products, the shear stress induced by the medium flow, and the retention of ECM components (32).

AIM OF THE PROJECT

An ever increasing number of studies focuses on the development of *in vitro* models more closely resembling their *in vivo* counterparts, bridging the gaps between developmental biology and precision medicine. While the organoid approach remains very promising, the use of liver organoids on a large scale needs to overcome the current technological and biological challenges of controlling organoid size, cell composition and shape.

The many progresses made in setting up 3D culture conditions, by monitoring and controlling specific environmental factors using bioreactors, provide new and better technologies to meet the reproducibility requirements.

In this view, our work aimed at the development of human liver organoids as a reliable 3D model for disease modeling and drug screening.

Our primary goal was to set up and optimize the protocols used to obtain organoids in a reproducible way and characterize them. Moreover, we cultured the organoids in either 3D dynamic and static culture conditions; studying their effects on the cells and identifying the culture condition with the best outcomes in terms of cell viability and behaviour.

In order to do so, we used a perfusion bioreactor: the IVTech's LiveBox1.

The LiveBox1 is a small bioreactor, comparable in sizes to classical culture-ware such as petri dishes and multiwell plates, allowing the use of a lower number of cells and smaller volumes of culture medium, when compared to other bioreactors, a crucial point when working with cells differentiated from iPSCs.

MATERIALS AND METHODS

CELL CULTURE

HFF

Human Foreskin Fibroblasts (HFF; provided by American Type Culture Collection, catalogue #CRL-2429) were maintained in Dulbecco's modified Eagle's medium (DMEM) (Thermo Fisher Scientific) supplemented with 15% fetal bovine serum (FBS, Thermo Fisher Scientific), 1% non-essential amino acids (Thermo Fisher Scientific), and 1% penicillin/streptomycin (Thermo Fisher Scientific).

Cells were passaged using Trypsin-EDTA (0.25%) (Thermo Fisher Scientific) every 3 or 4 days and split 1:4, with medium changes every other day.

Hep G2

Human hepatoma cells (Hep G2) (provided by American Type Culture Collection, catalogue #HB-8065) were maintained in Dulbecco's modified Eagle's medium (Thermo Fisher Scientific) supplemented with 10% FBS (Thermo Fisher Scientific), 1% non-essential amino acids (Thermo Fisher Scientific), and 1% penicillin/streptomycin (Thermo Fisher Scientific). Cells were trypsinized every 3 or 4 days and split 1:4, with medium changes every other day.

HUVECs

Human umbilical vein endothelial cells (HUVECs) were isolated from human umbilical cords, used at early (I–IV) passages, and grown on plastic culture-ware coated with 0.1% porcine gelatin (Merck) in Clonetics® EGM™-2 medium (Lonza). Cells were trypsinized every 3 or 4 days and split 1:4, with medium changes every other day. HUVECs were obtained from pregnant women, in accordance with the protocol approved by the Ethics Committee of Brescia (protocol number 1842).

iPSCs

Human Induced Pluripotent Stem Cells (iPSCs), Gibco Episomal hiPSC Line (cat#A18945) were bought from Thermo Fisher Scientific. They were seeded at a density of 15x10^3 cells/cm² and passaged every 3-4 days with daily medium changes. Briefly, iPSCs were detached using TryplE (Thermo Fisher Scientific), centrifuged at 300 g x 5 min and supernatant was discarded. Single cells were re-suspended in either mTeSR™1 or TeSR™E8™ (STEMCELL Technologies) in presence of 10μM of Rock Inhibitor Y-27632 (STEMCELL Technologies) and seeded on either Matrigel or rhLaminin-521 coated wells.

iPSCs were maintained on either a Matrigel® (Corning) or rhLaminin-521 (Thermo Fisher Scientific) coating. Matrigel® is maintained on ice and diluted in DMEM F-12 (Thermo Fisher Scientific), as per instructed on the datasheet, dispensed in the culture-ware and then incubated at 37° for 1 hour. rhLaminin-521 is diluted in PBS++ (Thermo Fisher Scientific) at a 0.5 μg/cm² concentration and left at 4°C overnight prior to use.

iMSCs

Mesenchymal progenitors were derived from iPSCs using the STEMdiff™ Mesenchymal Progenitor Kit (STEMCELL Technologies).

Briefly, on day -2 cells were detached and seeded in TeSR™E8™ at a density of 5x10^3 cells/cm² on a Matrigel® coated well. The medium was refreshed after 18-20 hours. On day 0, the medium was replaced with STEMdiff™ Mesenchymal Induction Medium and refreshed daily on days 1-3. On days 4-5 the medium was replaced with MesenCult™-ACF Plus Medium. On day 6 the cells were harvested, resuspended in MesenCult™-ACF Plus Medium with 10μM of Rock Inhibitor Y-27632 and seeded at a density of 1.5-10x10^3 cells/cm² on culture-ware coated with either Animal Component-Free Cell Attachment Substrate (STEMCELL Technologies) or 0.1% porcine gelatin.

Medium was refreshed every 2-3 days and the induced Mesenchymal Stem Cells (iMSCs) were seeded directly on plastic after the second passage.

In order to further investigate our cells' properties, we differentiated them in osteocytes and adipocytes using commercially available kits.

i) To obtain the osteogenic differentiation of iMCs, cells were plated at a 5 x 10^3 cells/cm^2 density; after reaching a 60-80% confluence, medium was replaced with StemPro® Complete Osteogenesis differentiation medium (Thermo Fisher Scientific). The medium was changed every 3-4 days until bone matrix formation occurred (approximately 15-20 days).

ii) To obtain the adipogenic differentiation of iMCs instead, cells were plated at a 10 x 10^3 cells/cm^2 density; after reaching a 60 - 80% confluency, medium was replaced with StemPro® Complete Adipogenesis Differentiation Medium (Thermo Fisher Scientific) and was changed every 3 days. Adipogenic differentiation occurred in approximately 15 days, confirmed by the appearance of lipid vacuoles.

We stained the cells obtained after the above-mentioned differentiation processes with Alizarin Red S and Oil Red O, respectively. The cells were fixed in 10% formalin for 1 hour at room temperature and then washed with water and stained by:

i) Alizarin Red S: Alizarin Red S (Merck) was reconstituted in water, pH was adjusted to 4.1 - 4.3; the solution was added to the cell, incubated for 45 minutes, and then the cells were washed with distilled water.

ii) Oil red O: The Oil Red O (Merck) working solution was prepared by diluting the Oil Red O stock solution (reconstituted with 100% isopropanol) at a 6:4 ratio in water. A solution of 60% isopropanol was added and incubated for 2-5 minutes. Oil Red O working solution was added and incubated for 10 minutes. Wash steps were repeated till the complete removal of the dye.

HEPATIC DIFFERENTIATION: from iPSCs to endoderm and further to iHEP

On day 0, the iPSCs were detached and resuspended in mTeSR™1 with 10μM of Rock Inhibitor Y-27632 and plated at a density of 2.1 x 10^5 cells/cm² onto coated wells.

After 24 hours, on day 1, the medium was replaced with Medium 1, prepared by diluting both supplements MR and CJ in STEMdiff™ Endoderm Basal Medium at a 1 in 100 dilution.

On day 2, the medium was replaced with Medium 2, prepared by adding Supplement CJ to STEMdiff™ Endoderm Basal Medium at a 1 in 100 dilution and changed daily on days 3-5.

On days 6 and 8, the medium was replaced with Hepatocytes Specification Medium, consisting of RPMI, B27, 10 ng/ml FGF2, 20 ng/ml BMP4. From day 9, the cells were cultured in Hepatocyte Maturation Medium consisting in Clonetics® HCM™ (Lonza) supplemented with 5% FBS, 100nM Dexamethasone, 20 ng/ml Oncostatin M and 10 ng/ml HGF (STEMCELL Technologies). Induced Hepatocytes (iHEPs) were used on day 9 of differentiation.

SPHEROIDS

Hep G2 spheroids were obtained using EZSPHERE Microplate 96 Well (REPROCELL) by seeding 160'000 cells in each well on day 0. Cells were then cultured for 24-48h.

ORGANOIDS

i) Mixed cell cultures: since obtaining iHEPs and iMSC is an expensive and time consuming process, preliminary experiments were carried out using a "mock" version of the intended cell populations in order to develop and optimize cell culture conditions. For the mock mixed culture (mMC), Hep G2, HUVECs and HFFs were mixed together at a 10:7:2 ratio and resuspended in a mix of DMEM + 10% FBS and EGM2 at a 1:1 ratio. Thus, HFF were used as cellular model for mesenchymal cells, and Hep G2 cells as model for hepatic derived cells. For the mixed culture (MC), iHEPs, HUVECs and iMSCs were mixed together at a 10:7:2

ratio and resuspended in the mixed culture medium, consisting of EGM2 and HCM (supplemented with 5% FBS, 100nM Dexamethasone, 20 ng/ml Oncostatin M and 10 ng/ml HGF) at a 1:1 ratio.

ii) Organoids: in order to obtain organoids (ORGs), either EZSPHERE Microplate 96 Well or AggreWell™ Microwell Plates (STEMCELL Technologies) were used. The mixed culture was seeded in a well on day 0, cultured for 48 hours and the ORGs obtained were then used for further applications.

3D DYNAMIC CULTURE

Liveflow and LiveBox1 (LB1) (IVTech) were used to perform the ORGs' 3D dynamic culture. This system is composed of a peristaltic pump allowing the generation of a constant fluid flow inside the LiveBox1 culture chamber. This fluid flow can be set in a range varying from 100 to 450 ml/min. In our experimental conditions, fluid flow was fixed on 330 ml/min. ORGs were resuspended in a solution of 1.5% alginate in HEPES-NaOH 20mM (pH = 7.4); drops 1-2 mm wide were formed by dispensing the solution containing the ORGs in $CaCl_2$ with a syringe. The drops, containing a total of about 150-200 ORGs, were cultured for 96 hours in the bioreactor and then collected. A peristaltic pump (IVTech LiveFlow®) creates the flow. All IVTech bioreactor's components were autoclaved.

FLOW CYTOMETRY

The cells were detached and resuspended in a stain buffer (PBS++, 2% BSA). The antibodies were added and the cells were incubated at 4°C for 20 minutes. Samples were analyzed using FACSCanto™ flow cytometry (BD Bioscience).

HUMAN CD MOLECULES	FLUOROCHROME	MANUFACTURER
CD34	PE/Cy7	BIOLEGEND
CD73	PE	BIOLEGEND
CD90	APC	BIOLEGEND
CD105	PerCP/Cy5.5	BIOLEGEND
CXCR4	FITC	BIOLEGEND
CD117	FITC	BIOLEGEND

Table 1. Flow cytometry antibodies.

VIABILITY ASSAY

The CellTiter-Glo® 3D Assay (Promega) was used to assess the ORGs' viability. The ORGs were collected from the multiwell plate or the bioreactor, put in an opaque multiwell plate and an equal volume of CellTiter-Glo® 3D Reagent was added to the culture medium. The ORGs were incubated at room temperature for 25 minutes, and luminescence was recorded.
To determine the number of ORGs to read for each point, a calibration curve was made on a range from 4 x 10^3 to 320 x 10^3 cells. From 160 x 10^3 cells up, the signal was in overload, while the best results were obtained in the range 40 - 80 x 10^3 cells. Since each ORG is composed of approximately 2 x 10^3 cells, the viability assay was carried out using 30 ORGs (in tryple) for each point.

PROTEIN QUANTIFICATION

Quick Start™ Bradford Protein Assay (BioRad) was used for protein quantification. The ORGs were collected, resuspended in lysis buffer, and sonicated on ice 3 times for 5 seconds. The samples transferred to a multiwell plate and 1x dye reagent was added to each well. Samples were incubated at room temperature for 5 minutes and then the absorbance at 595 nm was measured with a spectrophotometer.

IMMUNOHISTOCHEMISTRY

The ORGs were collected, centrifuged and the supernatant was discarded. A compacting solution consisting of 75% methanol, 20% chloroform and 5% glacial acetic acid was added to the pellet and let dry for 30 minutes. The pellet was stained with hematoxylin and eosin, in order to make it visible for the subsequent slicing, put in an histology cassette and fixed in 4% formaldehyde. The samples were then processed for inclusion. The 2 mm thick representative sections from paraffin embedded blocks were de-waxed and rehydrated. Endogenous peroxidase activity was blocked with 0.3% H2O2 (Sigma Aldrich) in methanol for 20 minutes. Antigen retrieval was performed using a microwave oven in 1.0 mM EDTA (Carlo Erba) buffer (pH 8.0) or in 1.0 mM Citrate (Carlo Erba and Panreac) buffer (pH6.0).

Sections were then washed in tris-buffered saline (TBS, Carlo Erba) (pH 7.4) and incubated for one hour in the specific primary antibody diluted in TBS 1% bovine serum albumin (BSA, Merck) (CD31 (clone PECAM-1) NovocastraTM 1:50), Alpha Fetoprotein (rabbit polyclonal, Diagnostic Biosystems, 1:200), CD90/Thy1 (rabbit monoclonal clone EPR3133, Abcam,1:50) and Vimentin (mouse monoclonal clone VP, Leica, 1:150).

The signal was revealed using the DAKO Envision+System-HRP Labelled Polymer Anti-Mouse or Anti-Rabbit, followed by diaminobenzydine (DAB) as chromogen and hematoxylin as counterstain. Images were acquired with a Nikon DS-Ri2 camera (4908 x 3264 full-pixel) mounted on a Nikon Eclipse 50i microscope equipped with Nikon Plan lenses (x10/0.25; x2070.40; x40/0.65; x100/1.25) using NIS-Elements 4.3 imaging software (Nikon Corporation).

IMMUNOSTAINING

Cells were fixed in 4% Immunofix (Bio-Optica) for 15 minutes and then permeabilized for 10 minutes with 0.1% Triton X-100 in PBS.

The cells were then incubated with Blocking Buffer (PBS containing 1% BSA, 2% Donkey serum (Thermo Fisher Scientific), 0.1% Triton X-100 (Merck)) for 60

minutes at room temperature. Next, primary antibodies (Table 2) diluted in blocking buffer were added and incubated 3 hours at room temperature. After washing, Alexa Fluor 594- and/or Alexa Fluor 488-conjugated secondary antibodies (ThermoFisher Scientific) were added 1 hour at room temperature. Cellular nuclei were stained with DAPI(Merck). The cells were observed under an inverted fluorescent microscope (Axiovert, Zeiss).

Antibody	**Company Cat#**
Mouse anti-SOX17	ThermoFisher Scientific, Cat#MA5-24885
Rabbit anti-FoxA2	ThermoFisher Scientific, Cat#720061
Rabbit anti-HNF4A	ThermoFisher Scientific, Cat#MA5-14891
Donkey anti-mouse IgG 488	ThermoFisher Scientific, Cat#A21202
Donkey anti-rabbit 488 IgG	ThermoFisher Scientific, Cat#A21206

Table 2. Immunostaining antibodies.

RNA EXTRACTION AND RT-PCR ANALYSIS

ORGs were homogenized prior to RNA extraction using a Micro-Vasoter Elvehjem 0,1 ml Wheaton potter (Biosigma).

Total RNA was extracted with Quick-RNA MiniPrep (Zymo Research), and then quantified.

Reverse transcriptase-PCR of 1 μg of total RNA was carried out using iScript cDNA Synthesis Kit (BIO-RAD), followed by specific PCR amplification. Sequences of individual primer pairs are detailed in Table 3.

GENE	**FORWARD/REVERSE (5'-3')**
OCT 3/4	GGGTTTTTGGGATTAAGTTCTTCA/GCCCCCACCCTTTGTGTT
SOX2	CAAAAATGGCCATGCAGGTT/AGTTGGGATCGAACAAAAGCTATT
NANOG	AGGAAGACAAGGTCCCGGTCAA/TCTGGAACCAGGTCTTCACCTGT
ACTB	CACTCTTCCAGCCTTCCTTC/AGTGATCTCCTTCTGCATCCT
HNF4a	TGCGACTCTCCAAAACCCTC/TGATGGGGACGTGTCATTGC
AFP	AAGTTTAGCTGACCTGGCTACC/TGCAGCAGTCTGAATGTCCG

ALB	TCTTCTGTCAACCCCACACG/GCAACCTCACTCTTGTGTGC
SERPINA1	TCCGATAACTGGGGTGACCT/AGACGGCATTGTCGATTCACT

Table 3. Primers.

SECRETED PROTEINS QUANTIFICATION

The secretion of Alpha-1 Antitrypsin (AAT), Alpha Fetoprotein (AFP), Aspartate Transaminase (AST), Alanine Transaminase (ALT) and Alkaline Phosphatase (AP) was measured in a collaboration with the *Laboratorio Centrale di Analisi Chimico-Fisiche of Spedali Civili di Brescia*. The iHEPs' culture medium was collected every other day starting from day 11 of differentiation.

Albumin quantification was carried out using the RayBio® Human Albumin ELISA Kit. Briefly, the medium of iHEPs at day 19 of differentiation was collected and diluted 500,000 fold in Assay Diluent C. The standard curve was prepared using the human Albumin provided with the kit.

Each standard and sample was added to the appropriate well and incubated for 2.5 hours at room temperature. The solution was then discarded and the wells were washed with 1X Wash solution. After the last wash, the plate was inverted and blotted against a clean paper towel. The biotinylated antibody was added to each well, incubated for 1 hour at room temperature. A wash step was repeated and then Streptavidin solution was added and incubated for 45 minutes at room temperature.

Another wash step was performed, TMB One-Step Substrate Reagent was added to each well and incubated for 30 minutes at room temperature.

The Stop Solution was then added to each well and the absorbance at 450 nm was immediately measured.

RESULTS

SPHEROIDS

To investigate the behaviour of cells in complex 3D systems, we directed our interest towards the development of a 3D organoid (ORG) model that could be further used in disease modeling and drug screening studies. “ORGs” are organ-like tissues obtained by mixing together multiple cell types in order to enhance their viability, engraftment potential, maturation status, etc.
Liver ORGs need an endothelial component, to help avoid necrosis at their inner core, and a stromal component, holding structural properties (14).
We started with setting up all the protocols needed for the actual ORGs’ formation using less valuable cell lines; indeed, the preliminary experiments were performed using Hep G2 hepatoma cells.
The first step of experiments consisted in finding a reproducible way to obtain spheroids (SPHs) that resemble the same 3D structure of an ORG, but are composed of a single cell type. Hep G2 cells were seeded and then cultured for 24-48 hours in peculiar multiwell plates, the EZSPHERE Microplate, which contain about 80 microwells for each of the 96 wells of the plate (Fig. 8). Each plate is individually laser-etched and coated with a biocompatible non-adherent surface so that the cells can slide to the bottom of the wells by gravity and hence aggregate forming SPHs.
After 48 hours, the SPHs were processed for inclusion; to optimize the protocol, we stained the pellet with hematoxylin and eosin in order to make it visible during the slicing. As shown in Fig. 9, there is only a small degree of variability in terms of size of the SPHs obtained: the average diameter size of the SPHs resulted being 161,6 μm, with a standard deviation of 52,8 (n= 30), thus validating the use of the EZSPHERE Microplates.

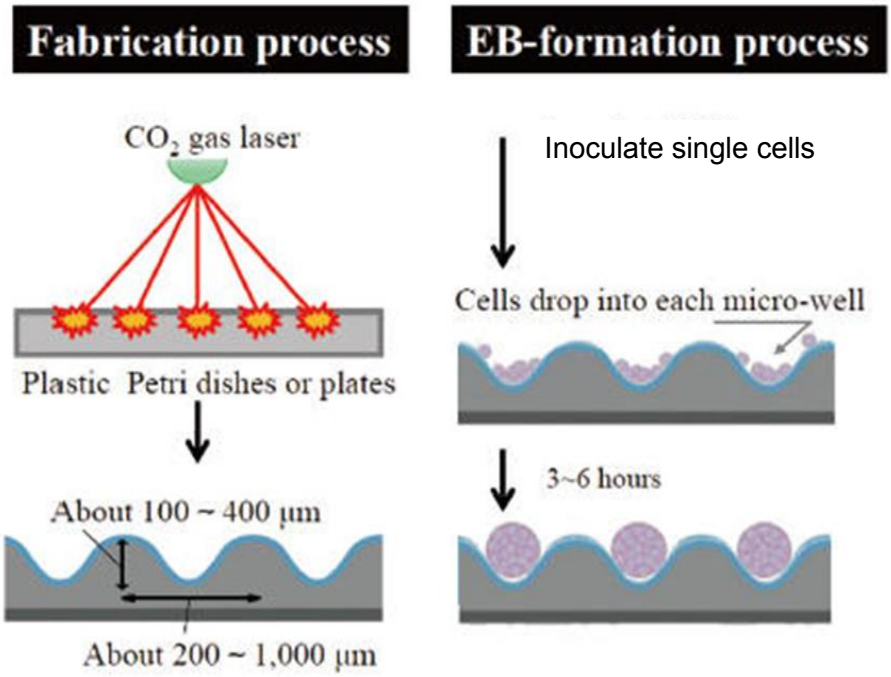

Figure 8. EZSPHERE Microplate's microwells (modified from EZSPHERE Microplate brochure).

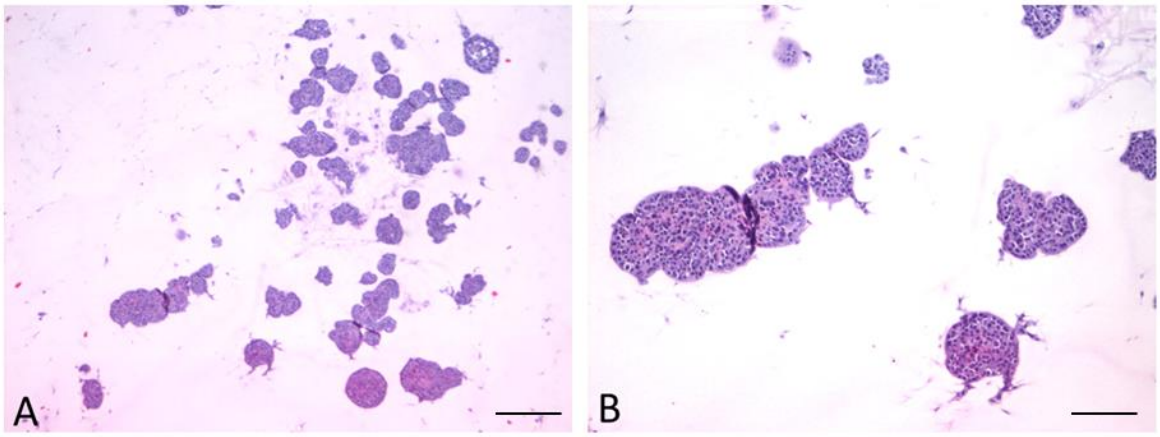

Figure 9. Hematoxylin and eosin staining for the SPHs. 4x magnification (A) and 10x magnification (B). Scale bar corresponding to 500 μm and 200 μm, respectively.

MOCK ORGANOIDS

Having identified a method to obtain SPHs/ORGs in a reproducible way, we proceeded to set up the remaining protocols using mock organoids (mORG), obtained by mixing together human hepatoma Hep G2 cells, human endothelial

cells HUVECs, and human fibroblasts HFFs as stromal component at a 10:7:2 previously published ratio (14); the mock mixed culture (mMC) was then grown for 48 hours (Fig. 10).

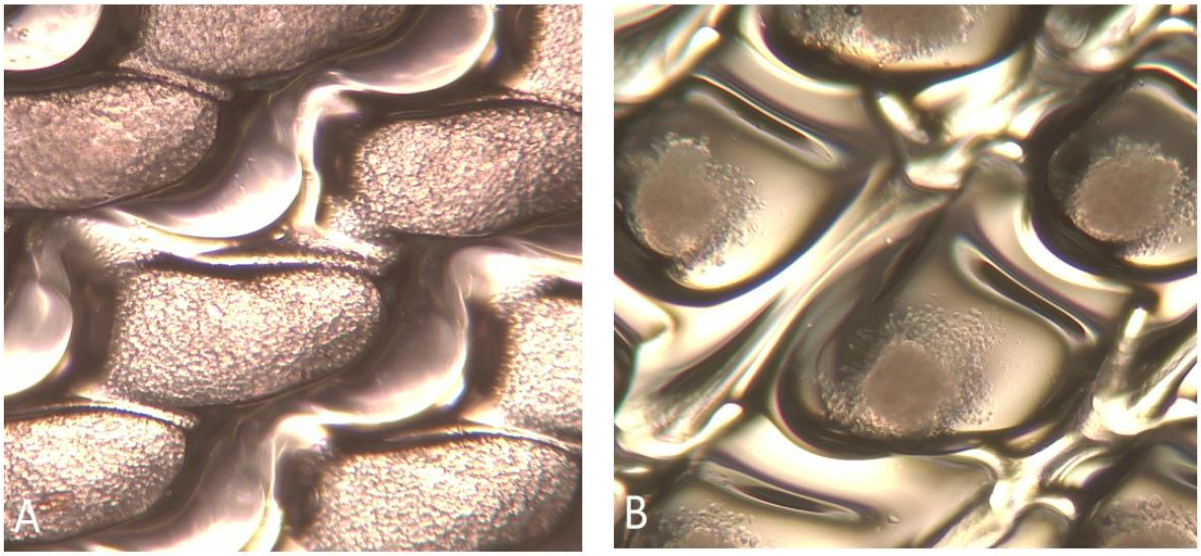

Figure 10. Cell seeding in the EZSPHERE Microplate. A shows the cells right after seeding, B shows the 3D cell agglomerates after 48 hours.

Since the size of the aggregates obtained reaches and exceeds 200 microns, a size considered problematic for the diffusion of nutrients in the cell culture medium, we compared the behaviour of the mORG in either static or dynamic culture conditions. LiveBox1 (LB1) was used to set up the mORG's 3D dynamic culture. LB1 (Fig. 11) is a transparent chamber designed for inter-connected dynamic cell cultures, featuring a flow inlet and outlet for the perfusion of cell culture media. The mORG were resuspended in a solution of 1.5% alginate and were entrapped in gel drops 1-2 mm wide by dispensing the suspension with a syringe in $CaCl_2$ solution (Fig. 12). The drops, containing a total of about 150-200 mORG, were cultured for 96 hours either in the bioreactor (Fig. 12B) or in a dish (Fig. 12A) and then collected. As a control culture we used the mORG grown statically in the EZ-SPHERE.

Figure 11. LiveBox1 chamber.

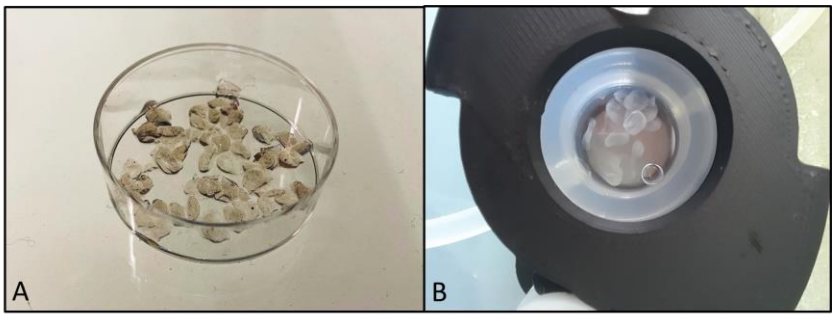

Figure 12. mORGs were incapsulated in alginate beads. These beads were maintained in either static (A) and dynamic (B) 3D culture conditions.

Fig. 13 shows the protocol setup:

- at T-2/D0, the mMC was seeded in the EZSPHERE;
- after 48 hours, at T0/D2 the mORGs were collected to perform a viability assay and to process for inclusion, and to set up all the different culture conditions;
- at Tf/D6, the experiment was stopped and all the samples were collected to perform further analysis.

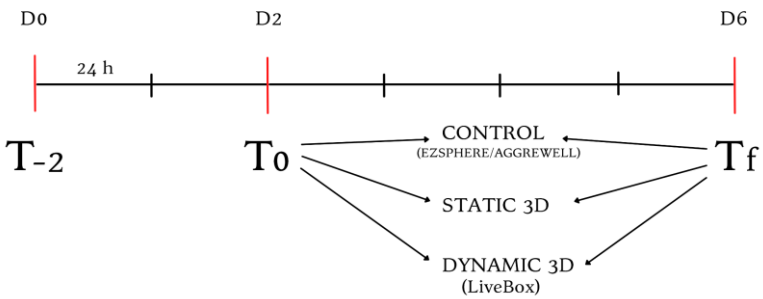

Figure 13. Protocol timeline and conditions of the experiment.

ANALYSIS OF mORG MORPHOLOGY

For a better understanding of the 3D morphology of the mORG, we embedded them in paraffin and stained them with hematoxylin and eosin (Fig. 14). In the mORGs' core we found some signs of necrosis, regardless of the culture condition (Fig. 14E-F), even if there seems to be a larger amount of dead cells in the control. We found that the ORGs cultured in the 3D static condition (Fig 14A) are larger than the other ones, even if they were all the same size at the starting point. A staining with a proliferation marker such as MIB1 will be necessary to see if their increase in size is due to proliferating cells.

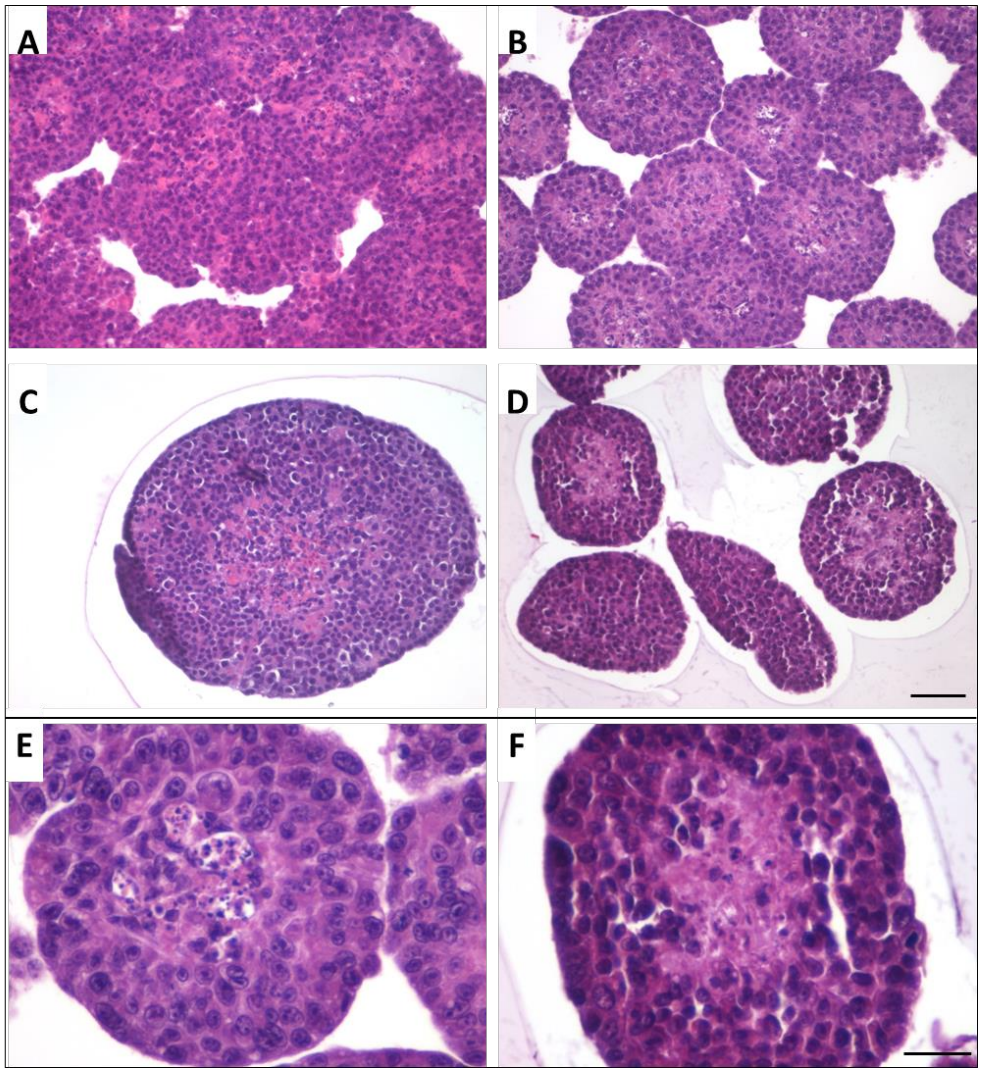

Figure 14. Hematoxylin and eosin staining for the mORG at To (A), Tf in EZSPHERE (B), static (C), and dynamic (D). Images are x20 original magnification, scale bar corresponding to 100 µm. 40x original magnification of representative necrotic core (E-F). Scale bar 50 µm.

To understand how the mORG self-assembled, we stained them for specific cell-lineage markers: CD31 for the endothelial cells, Alpha Fetoprotein (AFP) for the Hep G2, CD90/Thy1 and Vimentin for the fibroblasts. Fig. 15 shows that the core of the mORG is composed of HUVECs and fibroblasts, with an outer layer of Hep G2.

Moreover, there is a loss of AFP+ cells in the control condition (Fig. 15B) that could be due to either a loss of Hep G2 or to a switch in phenotype in such cells. This result needs to be further analyzed to fully comprehend it.

In addition, there's a high number of CD90+ cells in the static 3D culture condition (Fig. 15M), indicating that the CD90+ cells proliferated in this condition, whereas the weak vimentin signal could be explained by a phenotypical switch in the fibroblasts.

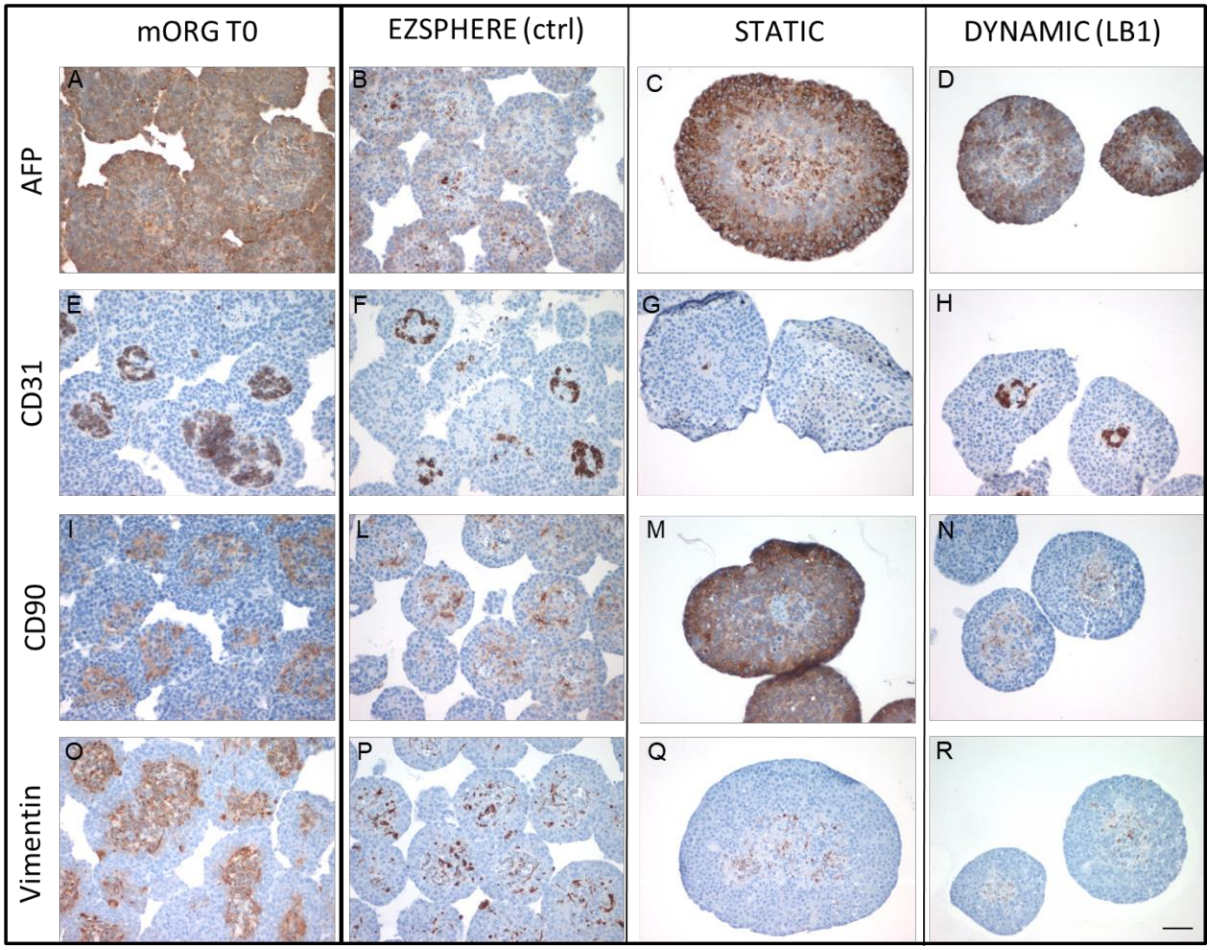

Figure 15. A-D staining for Alpha Fetoprotein on for the mORG at To (A), Tf in EZSPHERE (B), static (C), and dynamic (D). E-H staining for CD31 for the mORG at To (E), Tf in EZSPHERE (F), static (G), and dynamic (H). I-N staining for CD90 for the mORG at To (I), Tf in EZSPHERE (L), static (M), and dynamic (N). Staining for vimentin for the mORG at To (O), Tf in EZSPHERE (P), static (Q), and dynamic (R). All images are x20 original magnification, scale bar corresponding to 100 µm.

ASSESSMENT OF CELL VIABILITY in mORG

To assess the viability of the mORG, we used the CellTiter-Glo® 3D; this assay is specifically designed for determining cell viability in 3D microtissues, measuring ATP as an indicator of viability through a luminescent readout; the luciferase reaction for this assay is shown in Fig. 16.

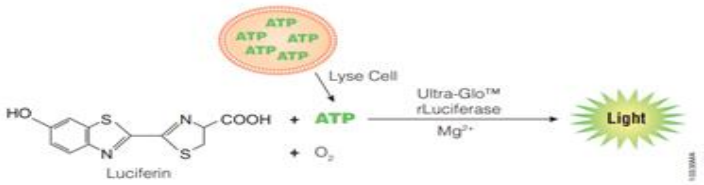

Figure 16. Luciferase reaction.

We quantified the amount of proteins in each sample and used it to normalize the luminescent data obtained (Fig. 17).

This is a necessary step because there's a small degree of variability among the ORGs' sizes. The data is therefore expressed in RLU/mg of protein. As shown in the chart in Fig. 17, there's a decrease of viable cells in the control culture condition, compared to the starting point, while the mORG cultured in the bioreactor show the highest viability, confirming our previously obtained data.

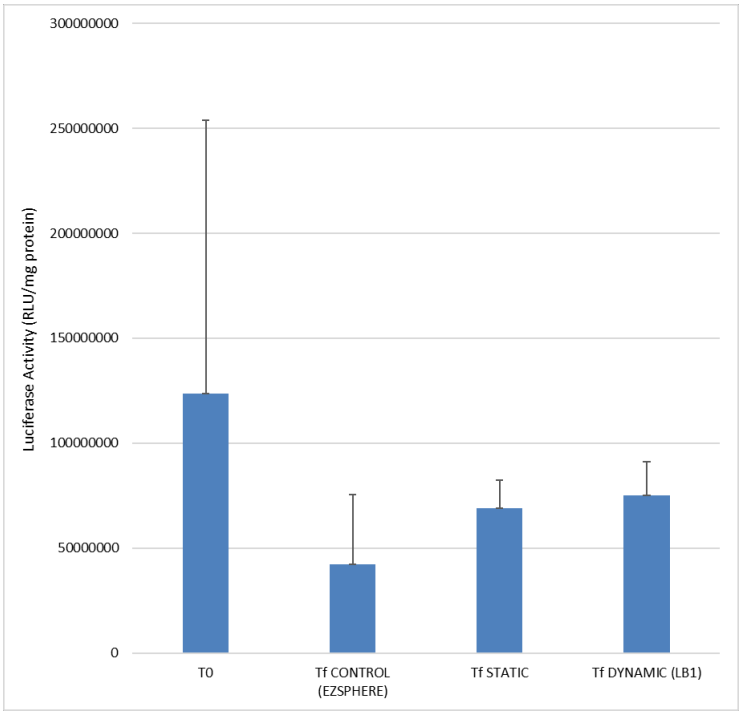

Figure 17. Luciferase activity (RLU/mg protein) at the starting point (To) and at the end point (Tf) for mORGs maintained is EZSPHERE, or static and dynamic culture conditions.

From this chart we can confirm that 3D culture conditions favor cell survival, even if we need more experiments to assess if the differences shown are statistically significant.

Having obtained these preliminary results and having set up our protocols, we then proceeded to derive mesenchymal stem cells (iMSCs) and hepatocytes (iHEPs) from a commercial iPSCs line used in our laboratory.

CELL DIFFERENTIATION AND CHARACHTERIZATION

iMSC

A high number of factors are involved in the formation of a 3D liver bud, including the fine regulation of signals between endodermal epithelial, mesenchymal and endothelial progenitors (10).
The mesenchymal component of our ORGs, crucial for the structural development, was derived from iPSCs.
We differentiated iMSCs from a control line used in our laboratory and then we performed a characterization of the cells obtained to assess their nature.
The International Society for Cellular Therapy (ISCT) defines MSCs on a set of characteristic properties:

- Plastic-adherent properties,
- Self-renewal capacity,
- Multi-lineage differentiation potential (e.g., osteocytes, adipocytes, and chondrocytes),
- Characteristic cell surface marker expression.

As shown in Fig. 18, after a week of differentiation we obtained mesenchymal looking cells that had self-renewal capacity and did adhere to plastic.

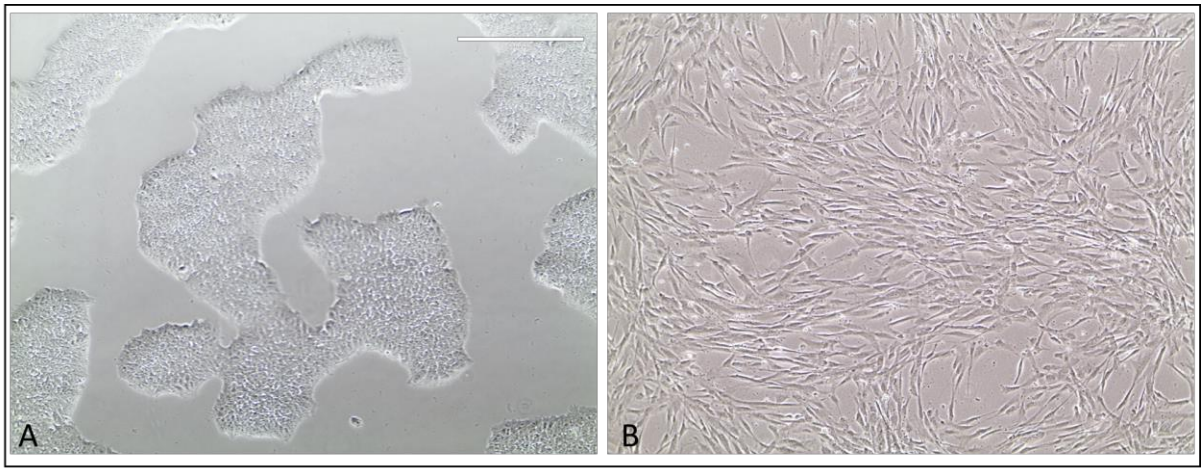

Figure 18. iPSCs colonies (A) and iMSCs (B) after one week of differentiation. Scale bar 400 µm.

We then tested the cells for the surface markers CD34, CD73, CD90 and CD105 using flow cytometry (Fig. 19). Our results show that 98% of the cell population is CD34-, and 92% of the population is CD73+, CD90+ and CD105+, thus confirming the mesenchymal characteristic cell surface marker expression.

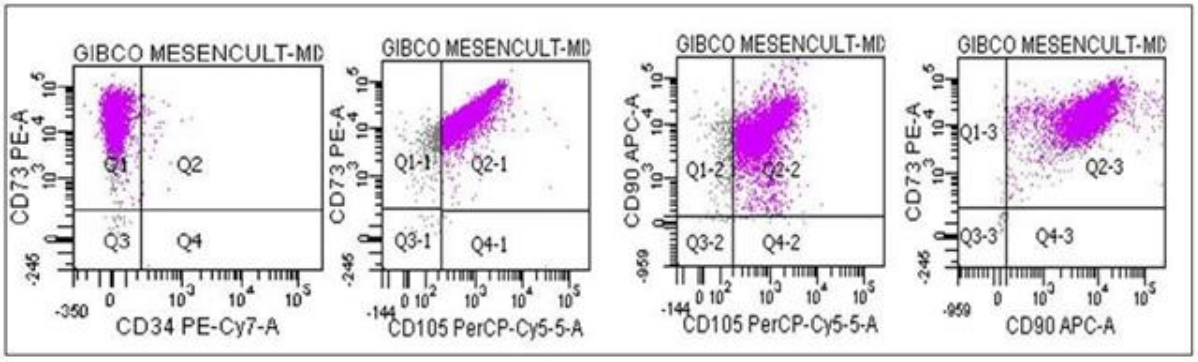

Figure 19. Flow cytometry analysis on iMSCs.

After 7 passages, we extracted the total mRNA from the cells and we measured the expression level of the pluripotency genes *OCT3/4*, *SOX2*, and *NANOG*. Fig. 20 shows that the pluripotency genes are downregulated in the differentiated cells, compared to the iPSC's expression level.

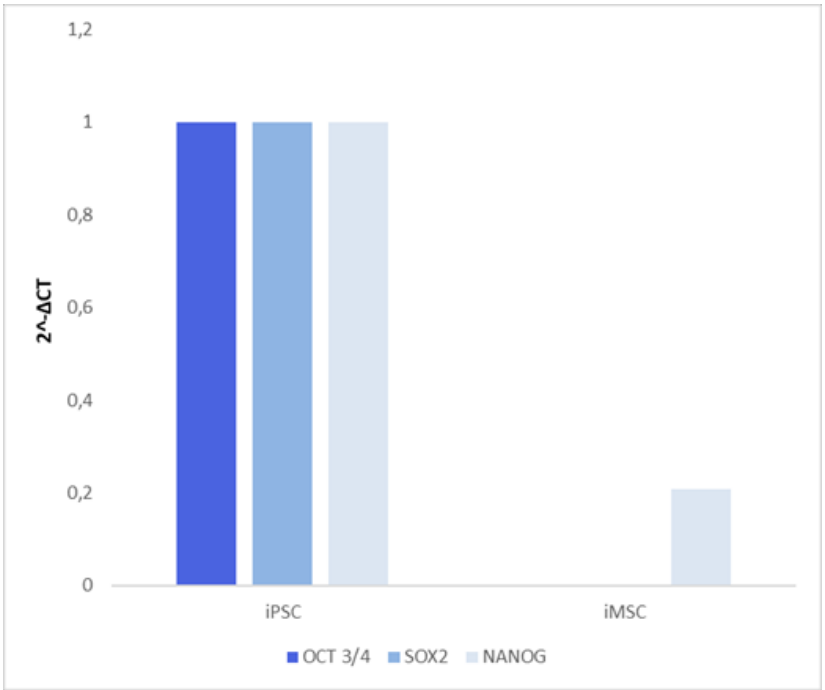

Figure 20. Expression level of the pluripotency markers OCT3/4, SOX2 and NANOG in iMSCs compared to iPSCs.

In order to further investigate our cells' properties, we differentiated them in osteocytes and adipocytes using commercially available kits; after 20 days of differentiation, we stained the cells obtained with Alizarin Red S and Oil Red O, respectively (Fig. 21).

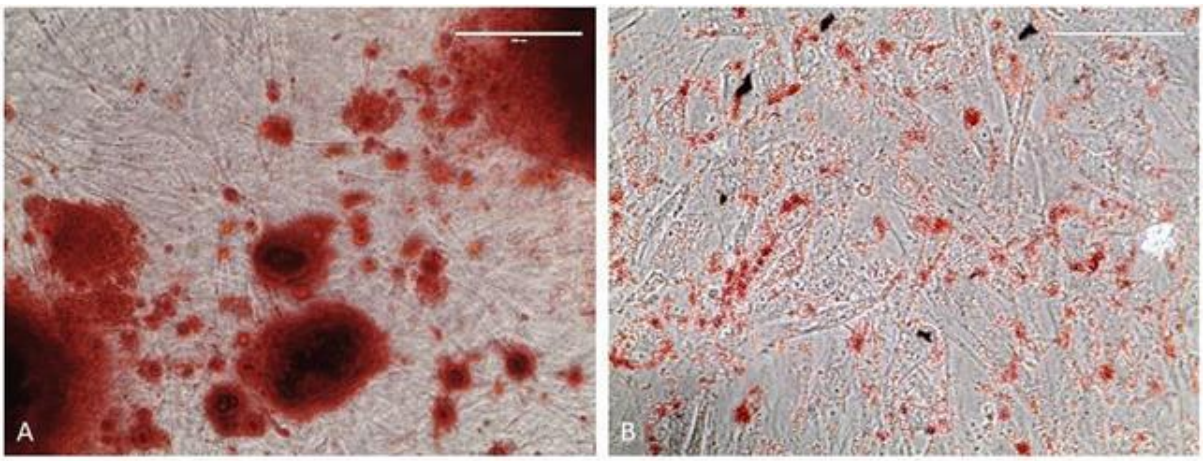

Figure 21. Staining with Alizarin Red S (A) and Oil Red O (B). Scale bar 400 µm.

Alizarin Red S reacts with calcium, thereby highlighting calcium deposits typical of osteocytes, while Oil Red O is a fat-soluble dye that stains neutral triglycerides and lipids. The positive staining for both of these dyes corroborates the multi-lineage differentiation potential of our cells.

These results taken together confirm that we successfully differentiated iMSCs from iPSCs that could be used for the next set of experiments.

iHEP

The core goal of our project was to assemble functional liver ORGs from patient derived iPSCs; for the set-up of the many protocols of our preliminary experiments, we used a control line.

The first step towards the derivation of hepatic lineage cells from iPSCs is the induction of definitive endoderm (DE) (Fig. 22); its efficiency can be monitored through the modulation of gene expression and/or changes in the expression of surface markers.

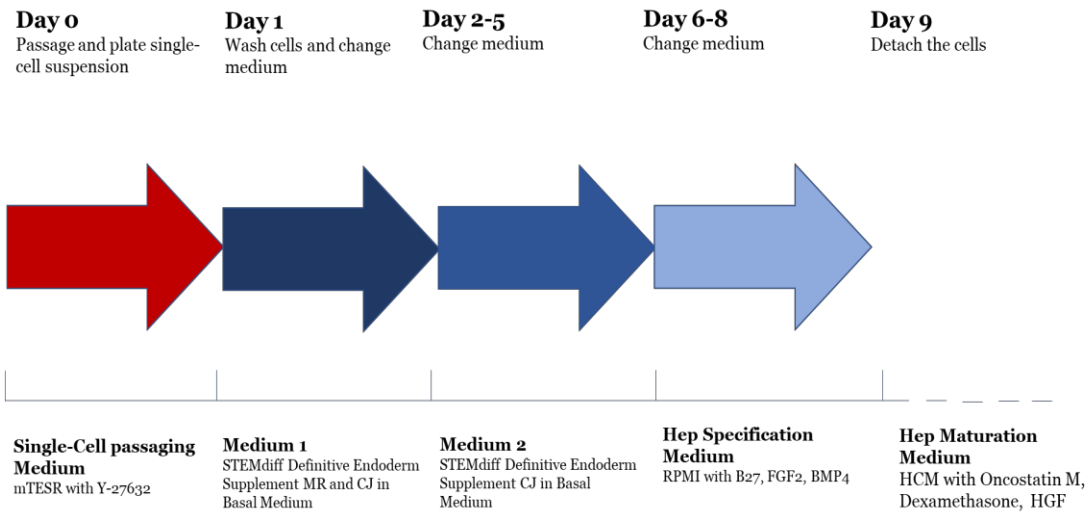

Figure 22. iHEPs' differentiation protocol.

The iPSCs were seeded at high density on Matrigel coated wells; after 24 hours the medium was replaced with STEMdiff™ Endoderm Basal Medium. At day 5 of differentiation, the cells show a change in morphology: the cells became larger,

flatter and acquired a polygonal shape, indeed resembling cells of endodermal origin (Fig. 23).

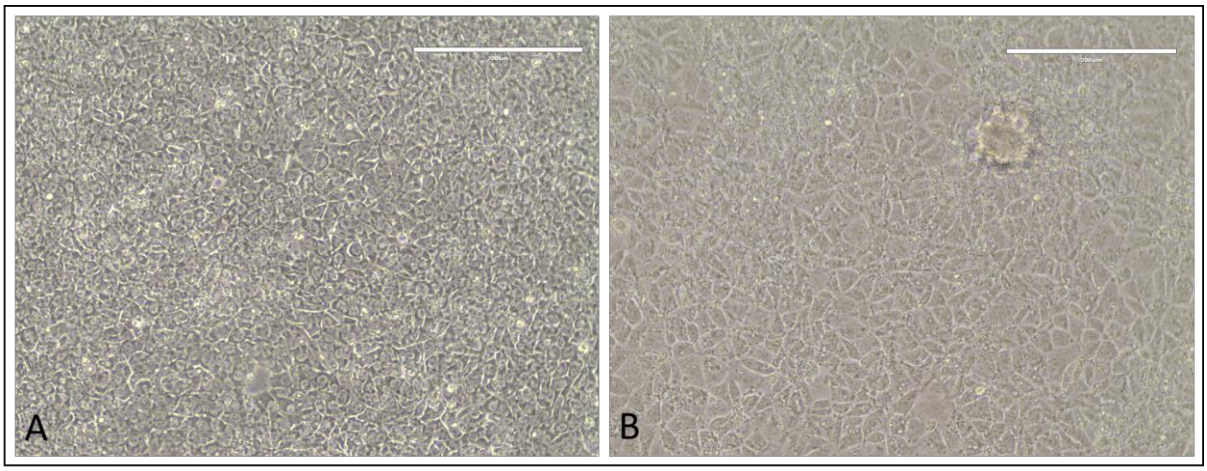

Figure 23. iPSCs cells 24 hours after seeding (A), definitive endoderm at day 5 of differentiation (B). Scale bar 200 µm.

Furthermore, on day 5 of differentiation, the cells obtained were analyzed by flow cytometry for the presence of CXCR4 and CD117, markers largely used to assess endoderm induction from iPSCs (Fig. 24). Our results show that 96.4% and 92.7% of the cell population is CXCR4+ and CD117+ respectively, from which we can confidently confirm the endodermal nature of the cells obtained.

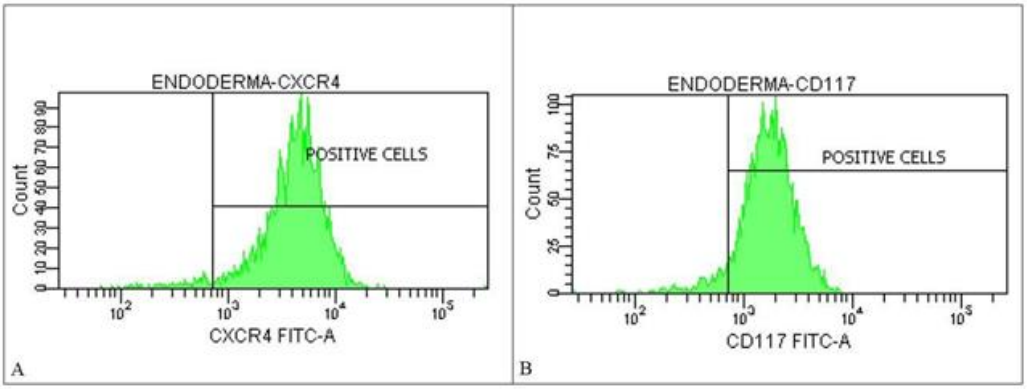

Figure 24. Flow cytometry analysis for CXCR4 (A) and CD117 (B).

To further characterize our cells, we stained them for another set of specific endodermal markers: FOXA2, a transcription factor involved in the development of multiple endoderm-derived organ systems such as the liver; HNF4, a transcrip-

tional regulator which controls the expression of hepatic genes during the transition of endodermal cells to hepatic progenitors; and SOX17, a transcription regulator which plays a key role in the regulation of embryonic development and is required for normal development of the definitive gut endoderm (9). Fig. 25 shows the expression of these markers in our cells, further confirming their endodermal nature.

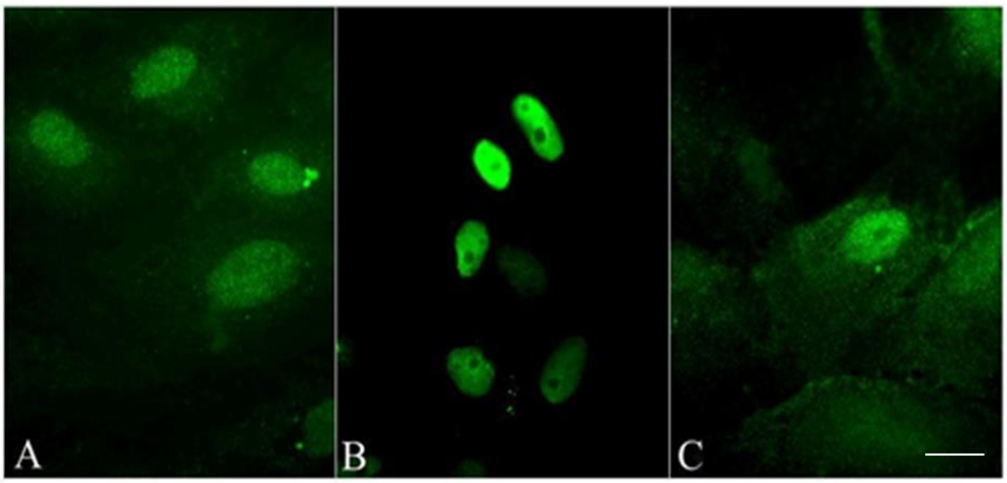

Figure 25. Staining for FOXA2 (A), HNF4 (B), SOX17 (C). Scale bar 20 μm.

We then proceeded to guide the hepatic specification by adding B27, bone morphogenetic protein (BMP-4) and basic Fibroblast Growth Factor (bFGF or FGF2) to the DE cell culture for additional two days. In order to promote maturation of the specified population, we cultured it in the presence of Hepatocyte Growth Factor (HGF), oncostatin M and dexamethasone for 15 days starting from day 9 of the differentiation.

At days 5 and 9 of differentiation, we extracted the total mRNA from the cells and we measured the expression level of the pluripotency genes *OCT3/4*, *NANOG,* key genes that are upregulated in iPSCs.

The histograms in Fig. 26 show that the pluripotency genes are downregulated in the differentiated cells, compared to the iPSCs' expression level.

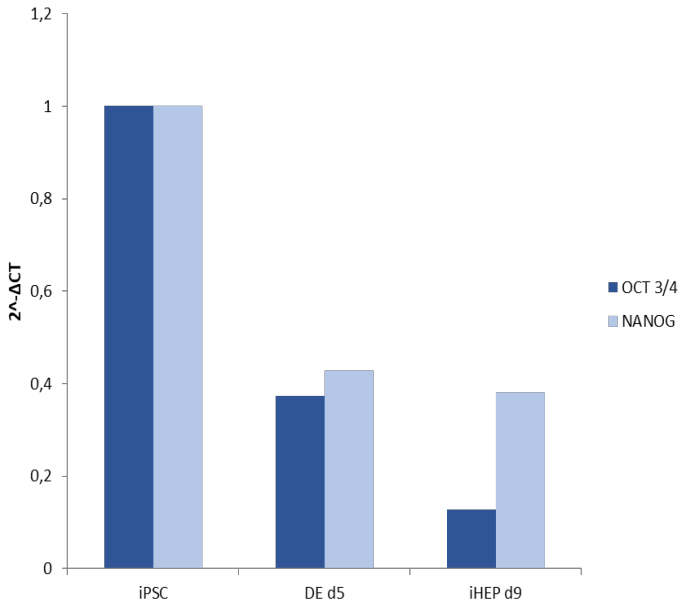

Figure 26. Expression level of the pluripotency markers OCT3/4 and NANOG in DE at day 5 of differentiation and iHEPs at day 9 of differentiation compared to iPSCs.

Moreover, the expression of *HNF4* is higher in the obtained cells compared to the iPSCs, and highest in the cells at day 9 of differentiation (Fig. 27).

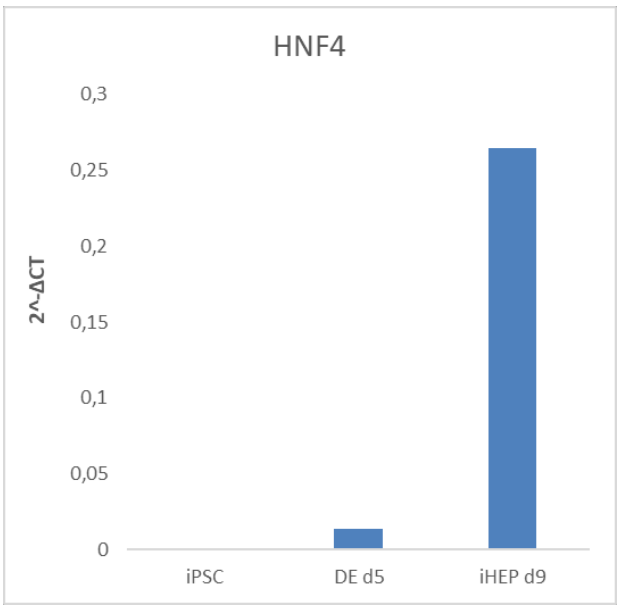

Figure 27. Expression level of HNF4 in DE at day 5 of differentiation and iHEPs at day 9 of differentiation compared to iPSCs.

These results confirm that the iPSCs were not only successfully differentiated into endodermal cells, but also that they achieved a more hepatocyte-like phenotype over time.

We also measured the expression of the *ALB*, *SERPINA1*, and *AFP*, confirming that these hepatic genes are not expressed in the iPSCs and furthermore, their expression is higher in the cells at day 9 of differentiation (Fig. 28).

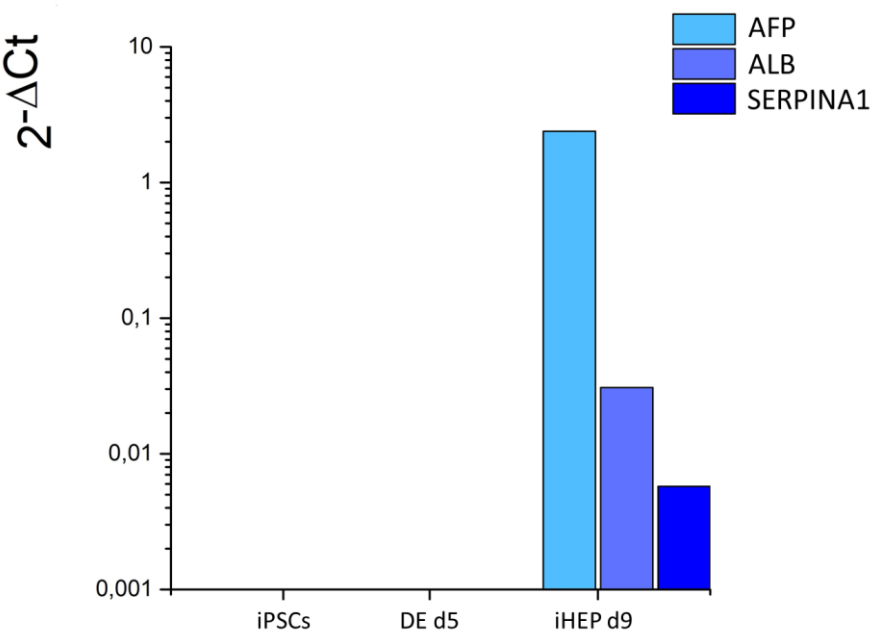

Figure 28. Expression level of AFP, ALB and SERPINA1 in DE at day 5 of differentiation and iHEPs at day 9 of differentiation compared to iPSCs.

We measured the secretion of several hepatic markers over time (day 11- day 23):

- Alpha-1 Antitrypsin (AAT), a protease inhibitor synthesized primarily by hepatocytes;
- Alpha Fetoprotein (AFP), marker of immature hepatocytes;
- Aspartate Transaminase (AST), which catalyzes the interconversion of aspartate and α-ketoglutarate to glutamate and oxaloacetate;
- Alanine Transaminase (ALT), which catalyzes the conversion of pyruvate and glutamate to L-alanine and a-ketoglutarate;
- Alkaline Phosphatase (AP), present in the canalicular membrane of the hepatocyte (Fig. 29).

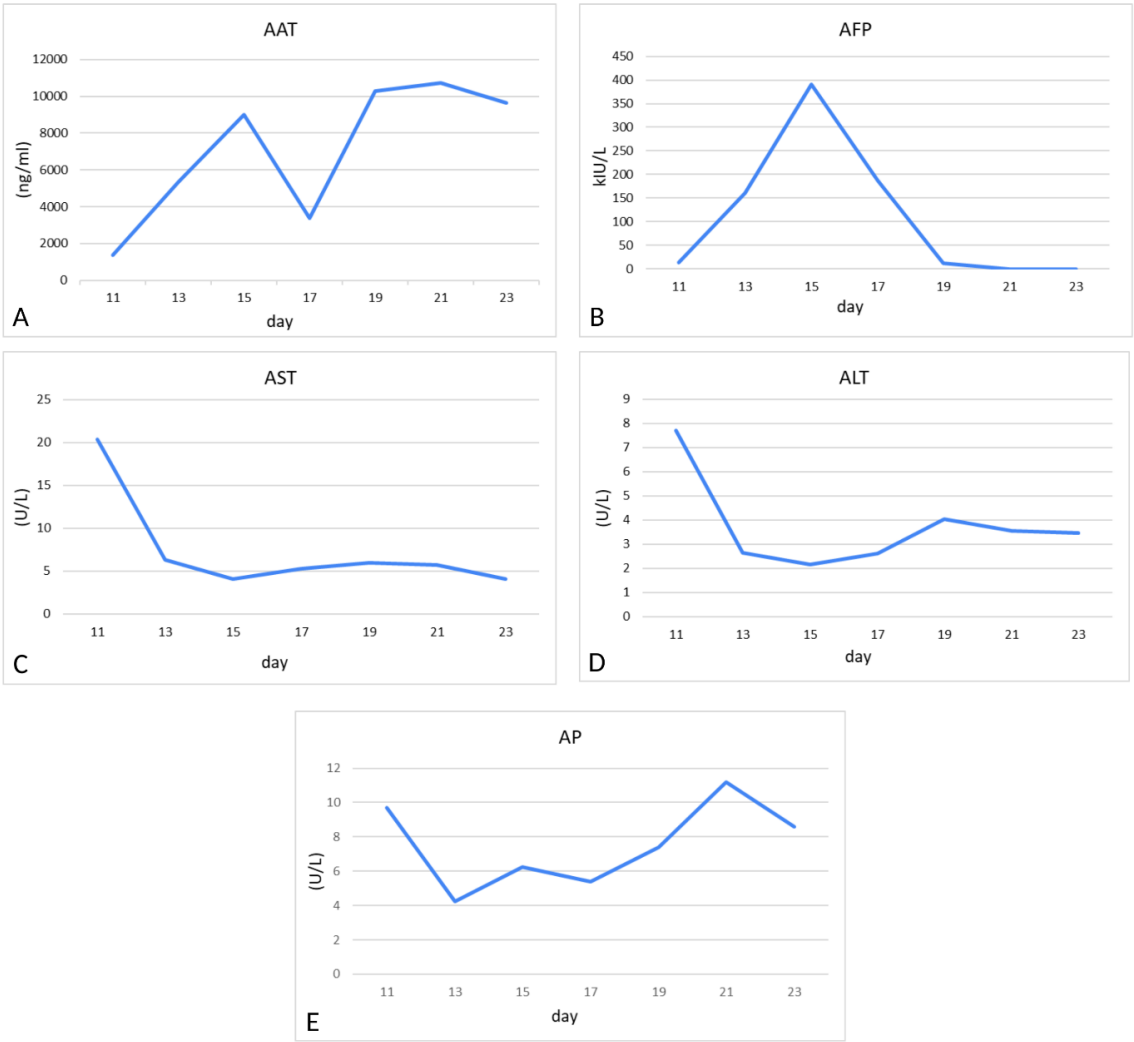

Figure 29. Quantification of AAT (A), AFP (B), AST (C), ALT (D), and AP (E) secretion.

This set of data confirms that the obtained cells secrete enzymes specific to the hepatocytes. More specifically, AST and ALT's secretion levels (Fig. 29C-D) are congruous with *in vitro* hepatocytes' secretion (38), while the secretion profile showed for AAT (Fig. 29A) has a very peculiar trend and needs to be deeply analyzed in further experiments.

These results suggest that between day 13 and 15 of differentiation a phenotypical change, probably towards a more mature status, occurs. We also hypothesize that the trend shown by AFP secretion (Fig. 29B) might depend on the different maturation status of the cells. In facts, during liver organogenesis in the embryo, the level of AFP expression decreases while ALB expression increases (35, 36), thus explaining the higher secretion of AFP at the early stage of hepatocyte differentia-

tion and its subsequent decrease at a later stage. Changes in the phenotype related to the maturation status might also explain the trend shown by AP's secretion levels (Fig. 29E), since iPSCs produce AP at their pluripotent stage (37) as do mature hepatocytes.

We also attempted to measure albumin (ALB) secretion, in a collaboration with the *Laboratorio Centrale di Analisi Chimico-Fisiche of Spedali Civili di Brescia*, but with this method we obtained a saturated signal. We therefore performed an ELISA assay on the medium collected from the culture at day 19 of the differentiation to assess the presence of ALB (Fig. 30A). Compared to primary human hepatocytes (39), iHEPs secrete less ALB; this could be due to a less mature phenotype. Nevertheless, these results show that our cells produce hepatic specific enzymes and proteins.

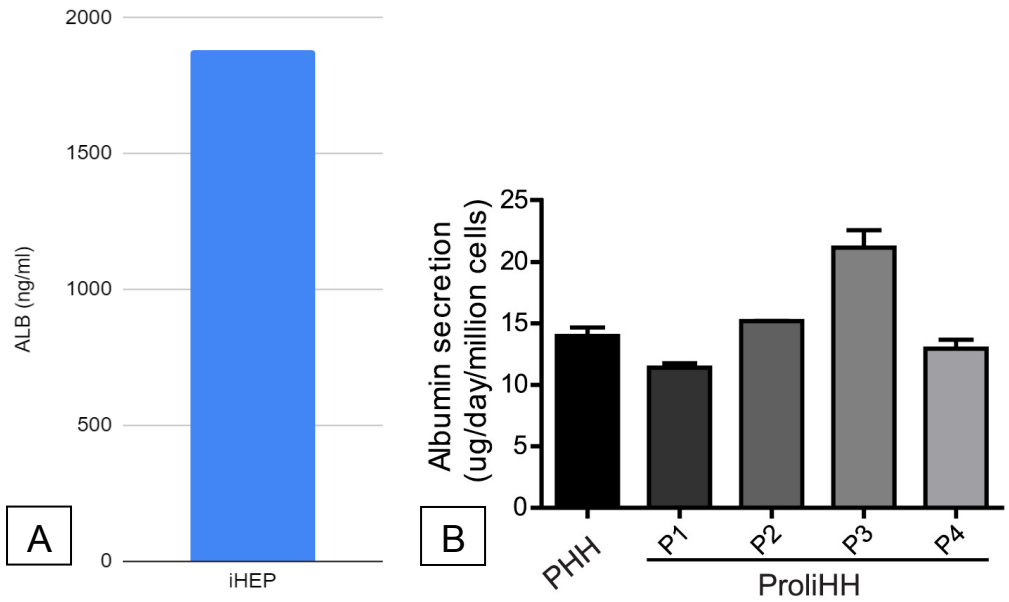

Figure 30. Quantification of ALB secretion in iHEP at day 19 of differentiation (A). ALB secretion in Proliferating Human Hepatocytes (ProliHH) in different passages (B) (Modified from Zhang et al., 2018)

ORGANOIDS

Having set up all the protocols and having successfully differentiated our cells of interest, we performed our experiments using iHEPs, HUVECs, and iMSCs mixed together at a 10:7:2 ratio (14). We cultured this mixed cell population (MC) for 48 hours in AggreWell™400 plates (Fig. 31); each well contains a standardized array

of microwells 400 µm in size, enabling the production of large numbers of embryoid bodies (EBs) and SPHs.

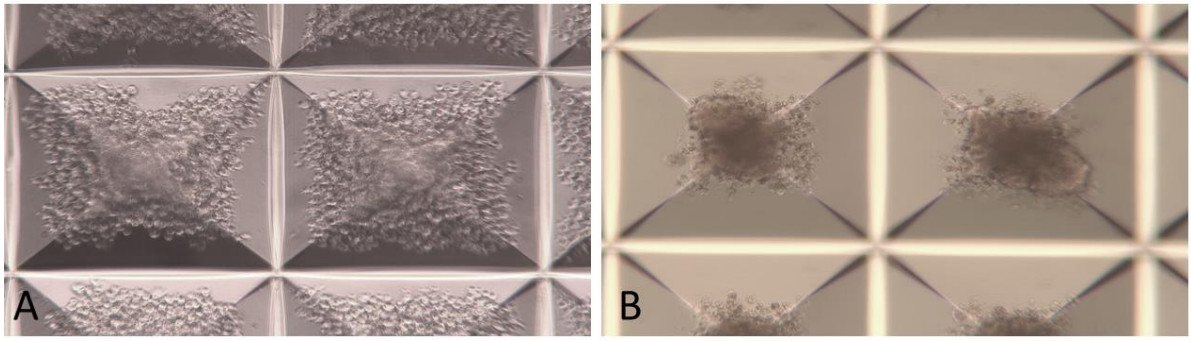

Figure 31. Cell seeded in the AGGREWELL plate. A shows the cells right after seeding, B shows the 3D cell agglomerates after 48 hours.

Since the differentiation of the iHEPs needed for the experiment requires millions of iPSCs, our first goal was to ensure that the actual ORGs could be grown in the previously set up conditions. In order to do so we carried out the experiment on a smaller scale: we used the time frame in Fig. 13, but without the LB1 culture condition.

The MC was seeded in the AGGREWELL plate at T-2 and after 48 hours (T0) we collected the ORGs, performed a viability assay, and set up the 3D culture condition. The ORGs were then cultured for an additional four days.

The viability assay (Fig. 32) confirmed that culturing the ORGs in a 3D static condition improved their viability, as previously shown in the preliminary experiments.

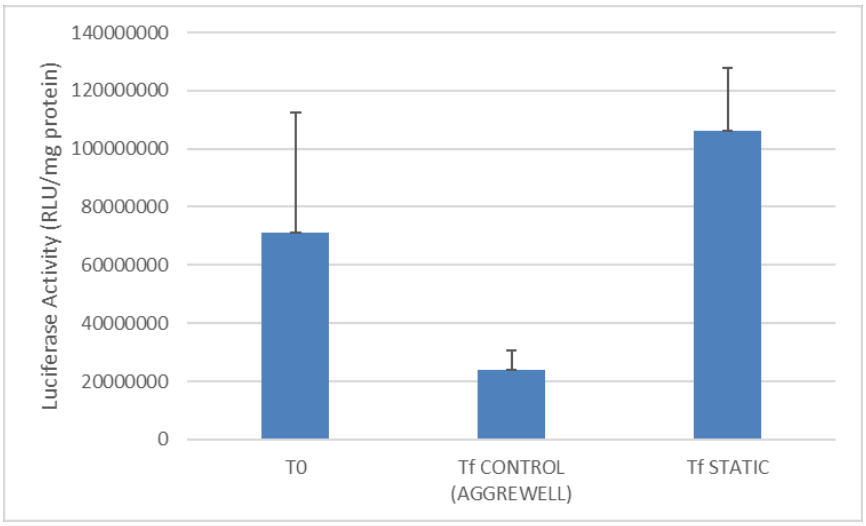

Figure 32. Luciferase activity (RLU/mg protein) at the starting point (T0) and at the end point (Tf) in the two different experimental conditions

To further investigate the ORGs' behaviour, we extracted the total RNA from the AGGREWELL samples at To and Tf, and measured the expression level of hepatic genes such as *ALB*, *SERPINA1*, and *AFP,* comparing them to samples of DE at day 5 of differentiation and iHEP at day 9 of differentiation. As shown in Fig. 33 there's an increased expression of *ALB*, *SERPINA1*, and *AFP* in the ORGs when compared to the single cell type population, which gets even higher at the experiment's end point for *ALB* and *AFP* (Fig. 33A, C); *SERPINA1*'s unique behavior will be further analyzed in following experiments. These results suggest that co-colturing iHEPs with iMSC and HUVEC might enhance their hepatic-like functions.

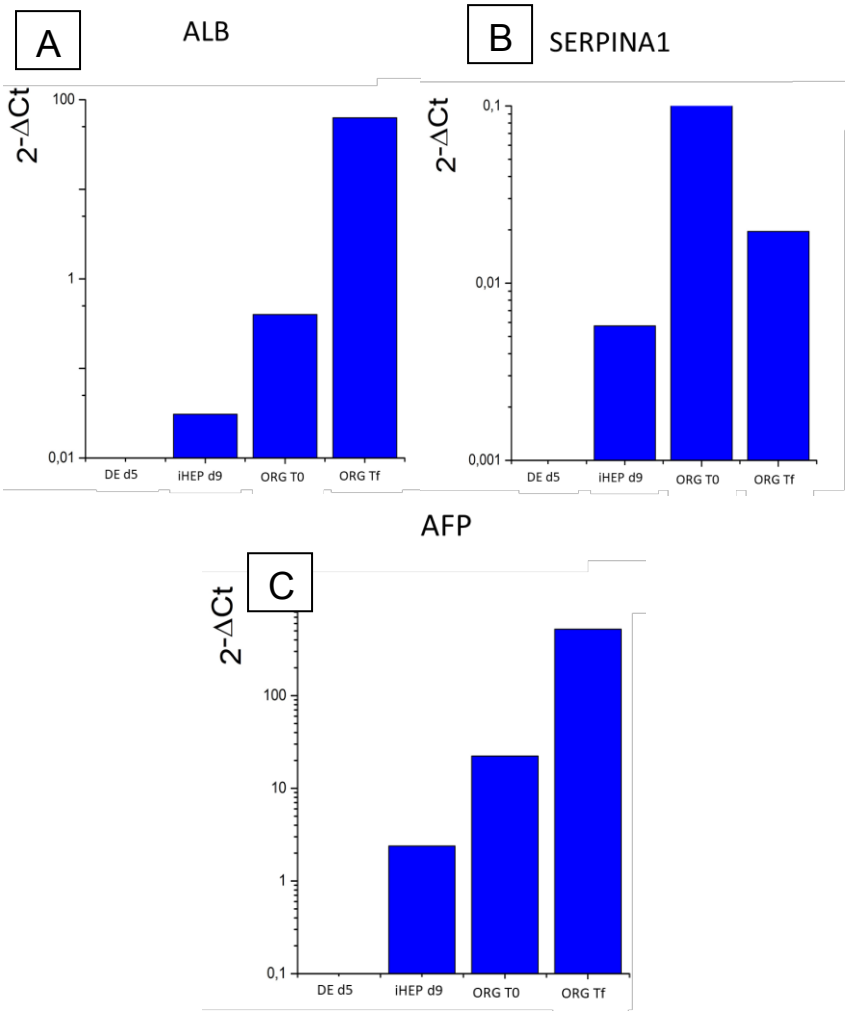

Figure 33. Expression level of ALB (A), SERPINA1 (B) and AFP (C) in the ORGs at the starting point (To) and at the end point (Tf) compared to DE at day 5 of differentiation and iHEPs at day 9 of differentiation.

Having obtained these results, we then proceeded to set up a more comprehensive experiment. We used the time frame of the previous experiments (Fig. 13), adding a 2D control condition: at T-2 the MC was seeded in both the AGGREWELL plate and in a standard 2D dish, maintaining the same ratio. Along with the MC, we performed the same experiments using only iHEPs (Fig. 34 and 35). Experiments and the analysis are still ongoing.

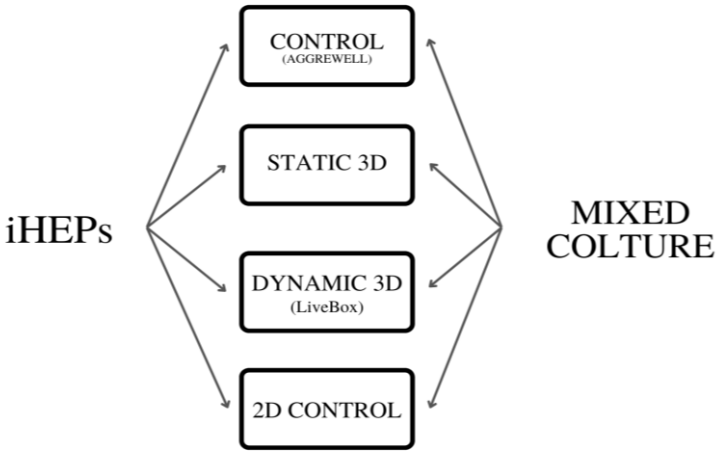

Figure 34. Experiment layout.

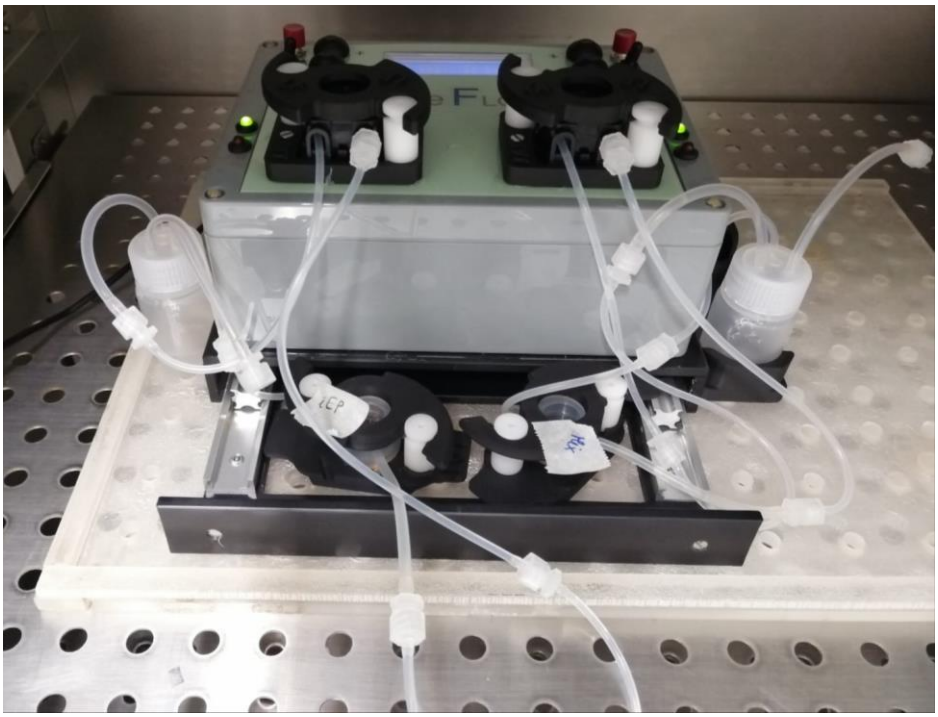

Figure 35. Parallel culture set up in the LiveBox1 bioreactor

CONCLUSION

Organoids are a powerful tool to apply in developmental studies, drug screening, and disease modeling. The ever increasing progress made in finding new technologies to obtain and culture 3D cell aggregates, makes this model more and more closely resembling its *in vivo* counterpart. The organoid model is therefore as promising as it can be a challenging technology.

The first challenge when assembling 3D constructs lies in making the process as reproducible as possible; we overcame this critical issue by using peculiar multiwell plates specifically designed to obtain 3D cell microaggregates. Not only using these multiwell plates granted an acceptable degree of variability in terms of size of the aggregates, but the high number of microwells on each plate easily allowed the production of a batch of spheroids/organoids.

Another challenging aspect of this technology is the search for the right culture conditions that not only give the best outcome in terms of viability, but also in terms of physiological behavior, especially when working with iPSCs-derived cells. The optimal culture condition should allow the organoids to reach the appropriate state of maturation, while maintaining their *in vivo* counterpart's functional properties.

In this view, a growing amount of studies on 3D constructs rely on bioreactors, since they allow to control in a precise and reproducible way the environmental conditions required for cell culture, such as temperature, pH, flow rate, oxygen, nutrient supply, and waste metabolite removal. However, the main limitation of classic bioreactors technology consists in the high number of cells needed for the culture, hence why we used the LiveBox1, a small bioreactor comparable in sizes to classical culture-ware such as petri dishes and multiwell plates.

In our preliminary study, we demonstrated that using a dynamic culture condition, such as the LiveBox1 bioreactor, increased the viability of the cultured organoids.

Our goal was to develop a model that could be used in disease modeling and drug screening tests, hence why we wanted to derive patient-specific cells.

Using a commercial iPSCs line we differentiated and characterized iMSCs and iHEPs to use to assemble the organoids. Both obtained cell types express characteristic markers and properties, thus confirming their nature.

Each experiment takes roughly 3-4 weeks of preparation time to obtain the necessary cells: only for the experiment in Fig. 34 we needed 12 x 10^6 iPSC to differentiate into 19 x 10^6 iHEPs just to perform the basic analysis: viability assay, morphology assessment and total RNA extraction; many characterization studies are yet to follow and still needed.

In conclusion, though setting up and optimizing a 3D organoid model can be challenging, the perks and possibilities this tool has to offer outweigh the efforts needed.

BIBLIOGRAPHY

1. Lancaster MA, Knoblich JA. Organogenesis in a dish: modeling development and disease using organoid technologies. Science. 2014 Jul 18;345(6194):1247125. doi: 10.1126/science.1247125. Epub 2014 Jul 17. PMID: 25035496.

2. Prior N, Inacio P, Huch M. Liver organoids: from basic research to therapeutic applications. Gut. 2019 Dec;68(12):2228-2237. doi: 10.1136/gutjnl-2019-319256. Epub 2019 Jul 12. PMID: 31300517; PMCID: PMC6872443.

3. Weiss P, Taylor AC. Reconstitution of complete organs from single-cell suspensions of chick embryos in advanced stages of differentiation. Proc Natl Acad Sci U S A. 1960 Sep;46(9):1177-85. doi: 10.1073/pnas.46.9.1177. PMID: 16590731; PMCID: PMC223021.

4. Steinberg MS, in Cellular Membranes in Development, M. Locke, Ed. (Academic Press, New York, 1964), pp. 321–366.

5. Agathocleous M, Harris WA. From progenitors to differentiated cells in the vertebrate retina. Annu Rev Cell Dev Biol. 2009;25:45-69. doi: 10.1146/annurev.cellbio.042308.113259. PMID: 19575661.

6. Huch M, Koo BK. Modeling mouse and human development using organoid cultures. Development. 2015 Sep 15;142(18):3113-25. doi: 10.1242/dev.118570. PMID: 26395140.

7. Orkin RW, Gehron P, McGoodwin EB, Martin GR, Valentine T, Swarm R. A murine tumor producing a matrix of basement membrane. J Exp Med. 1977 Jan 1;145(1):204-20. doi: 10.1084/jem.145.1.204. PMID: 830788; PMCID: PMC2180589.

8. Carlson BM. Human Embryology and Developmental Biology (5th ed). Philadelphia, PA: Elsevier, 2014

9. Zaret KS. Regulatory phases of early liver development: paradigms of organogenesis. Nat Rev Genet. 2002 Jul;3(7):499-512. doi: 10.1038/nrg837. PMID: 12094228.

10. Zorn AM. Liver development. 2008 Oct 31. In: StemBook [Internet]. Cambridge (MA): Harvard Stem Cell Institute; 2008–. PMID: 20614624.

11. Prior N, Inacio P, Huch M. Liver organoids: from basic research to therapeutic applications. Gut. 2019 Dec;68(12):2228-2237. doi: 10.1136/gutjnl-2019-319256. Epub 2019 Jul 12. PMID: 31300517; PMCID: PMC6872443.

12. Huch M, Dorrell C, Boj SF, van Es JH, Li VS, van de Wetering M, Sato T, Hamer K, Sasaki N, Finegold MJ, Haft A, Vries RG, Grompe M, Clevers H. In vitro expansion of single Lgr5+ liver stem cells induced by Wnt-driven regeneration. Nature. 2013 Feb 14;494(7436):247-50. doi: 10.1038/nature11826. Epub 2013 Jan 27. PMID: 23354049; PMCID: PMC3634804.

13. Huch M, Gehart H, van Boxtel R, Hamer K, Blokzijl F, Verstegen MM, Ellis E, van Wenum M, Fuchs SA, de Ligt J, van de Wetering M, Sasaki N, Boers SJ, Kemperman H, de Jonge J, Ijzermans JN, Nieuwenhuis EE, Hoekstra R, Strom S, Vries RR, van der Laan LJ, Cuppen E, Clevers H. Long-term culture of genome-stable bipotent stem cells from adult human liver. Cell. 2015 Jan 15;160(1-2):299-312. doi: 10.1016/j.cell.2014.11.050. Epub 2014 Dec 18. PMID: 25533785; PMCID: PMC4313365.

14. Takebe T, Sekine K, Enomura M, Koike H, Kimura M, Ogaeri T, Zhang RR, Ueno Y, Zheng YW, Koike N, Aoyama S, Adachi Y, Taniguchi H. Vascularized and functional human liver from an iPSC-derived organ bud transplant. Nature. 2013 Jul 25;499(7459):481-4. doi: 10.1038/nature12271. Epub 2013 Jul 3. PMID: 23823721.

15. Fagiuoli S, Daina E, D'Antiga L, Colledan M, Remuzzi G. Monogenic diseases that can be cured by liver transplantation. J Hepatol. 2013 Sep;59(3):595-612. doi: 10.1016/j.jhep.2013.04.004. Epub 2013 Apr 8. PMID: 23578885.

16. Kobelska-Dubiel N, Klincewicz B, Cichy W. Liver disease in cystic fibrosis. Prz Gastroenterol. 2014;9(3):136-41. doi: 10.5114/pg.2014.43574. Epub 2014 Jun 26. PMID: 25097709; PMCID: PMC4110359.

17. Dekkers JF, Wiegerinck CL, de Jonge HR, Bronsveld I, Janssens HM, de Winter-de Groot KM, Brandsma AM, de Jong NW, Bijvelds MJ, Scholte BJ, Nieuwenhuis EE, van den Brink S, Clevers H, van der Ent CK, Middendorp S, Beekman JM. A functional CFTR assay using primary cystic fibrosis intestinal organoids. Nat Med. 2013 Jul;19(7):939-45. doi: 10.1038/nm.3201. Epub 2013 Jun 2. PMID: 23727931.

18. Sampaziotis F, de Brito MC, Madrigal P, Bertero A, Saeb-Parsy K, Soares FAC, Schrumpf E, Melum E, Karlsen TH, Bradley JA, Gelson WT, Davies S, Baker A, Kaser A, Alexander GJ, Hannan NRF, Vallier L. Cholangiocytes derived from human induced pluripotent stem cells for disease modeling and drug validation. Nat Biotechnol. 2015 Aug;33(8):845-852. doi: 10.1038/nbt.3275. Epub 2015 Jul 13. PMID: 26167629; PMCID: PMC4768345.

19. Ogawa M, Ogawa S, Bear CE, Ahmadi S, Chin S, Li B, Grompe M, Keller G, Kamath BM, Ghanekar A. Directed differentiation of cholangiocytes from human pluripotent stem cells. Nat Biotechnol. 2015 Aug;33(8):853-61. doi: 10.1038/nbt.3294. Epub 2015 Jul 13. PMID: 26167630.

20. Kaplowitz N. Idiosyncratic drug hepatotoxicity. Nat Rev Drug Discov. 2005 Jun;4(6):489-99. doi: 10.1038/nrd1750. PMID: 15931258.

21. Corrò C, Novellasdemunt L, Li VSW. A brief history of organoids. Am J Physiol Cell Physiol. 2020 Jul 1;319(1):C151-C165. doi: 10.1152/ajpcell.00120.2020. Epub 2020 May 27. PMID: 32459504; PMCID: PMC7468890.

22. Freshney, IR. (2005) Culture of animal Cells. A Manual of Basic Technique, 5 ed. John Wiley & Sons, Hoboken, NJ.

23. Haycock JW. 3D cell culture: a review of current approaches and techniques. Methods Mol Biol. 2011;695:1-15. doi: 10.1007/978-1-60761-984-0_1. PMID: 21042962.

24. Pampaloni F, Reynaud EG, Stelzer EH. The third dimension bridges the gap between cell culture and live tissue. Nat Rev Mol Cell Biol. 2007 Oct;8(10):839-45. doi: 10.1038/nrm2236. PMID: 17684528.

25. Martin I, Wendt D, Heberer M. The role of bioreactors in tissue engineering. Trends Biotechnol. 2004 Feb;22(2):80-6. doi: 10.1016/j.tibtech.2003.12.001. PMID: 14757042.

26. Vunjak-Novakovic G, Freed LE, Biron RJ, and Langer R. (1996) Effects of mixing on the composition and morphology of tissue-engineered cartilage. AIChE J. 42, 850–860.

27. Sutherland RM, Sordat B, Bamat J, Gabbert H, Bourrat B, Mueller-Klieser W. Oxygenation and differentiation in multicellular spheroids of human colon carcinoma. Cancer Res. 1986 Oct;46(10):5320-9. PMID: 3756881.

28. Martin I, Obradovic B, Freed LE, Vunjak-Novakovic G. Method for quantitative analysis of glycosaminoglycan distribution in cultured natural and engineered cartilage. Ann Biomed Eng. 1999 Sep-Oct;27(5):656-62. doi: 10.1114/1.205. PMID: 10548335.

29. Carrier RL, Papadaki M, Rupnick M, Schoen FJ, Bursac N, Langer R, Freed LE, Vunjak-Novakovic G. Cardiac tissue engineering: cell seeding, cultivation parameters, and tissue construct characterization. Biotechnol Bioeng. 1999 Sep 5;64(5):580-9. doi: 10.1002/(sici)1097-0290(19990905)64:5<580::aid-bit8>3.0.co;2-x. PMID: 10404238.

30. Rhee HW, Zhau HE, Pathak S, Multani AS, Pennanen S, Visakorpi T, Chung LW. Permanent phenotypic and genotypic changes of prostate cancer cells cul-

tured in a three-dimensional rotating-wall vessel. In Vitro Cell Dev Biol Anim. 2001 Mar;37(3):127-40. doi: 10.1290/1071-2690(2001)037<0127:PPAGCO>2.0.CO;2. PMID: 11370803.

31. Licato LL, Prieto VG, Grimm EA. A novel preclinical model of human malignant melanoma utilizing bioreactor rotating-wall vessels. In Vitro Cell Dev Biol Anim. 2001 Mar;37(3):121-6. doi: 10.1290/1071-2690(2001)037<0121:ANPMOH>2.0.CO;2. PMID: 11370802.

32. Martin I, Wendt D, Heberer M. The role of bioreactors in tissue engineering. Trends Biotechnol. 2004 Feb;22(2):80-6. doi: 10.1016/j.tibtech.2003.12.001. PMID: 14757042.

33. Clevers H. Modeling Development and Disease with Organoids. Cell. 2016 Jun 16;165(7):1586-1597. doi: 10.1016/j.cell.2016.05.082. PMID: 27315476.

34. Langer R, Vacanti JP. Tissue engineering. Science. 1993 May 14;260(5110):920-6. doi: 10.1126/science.8493529. PMID: 8493529.

35. Lazarevich, N. L. (2000). Molecular mechanisms of alpha-fetoprotein gene expression. BIOCHEMISTRY C/C OF BIOKHIMIIA, 65(1), 117-133.

36. Zhao, R., & Duncan, S. A. (2005). Embryonic development of the liver. Hepatology, 41(5), 956-967.

37. Kuang, Y., Miki, K., Parr, C., Hayashi, K., Takei, I., Li, J., Iwasaki, M., Nakagawa, M., Yoshida, Y., & Saito, H. (2017). Efficient, Selective Removal of Human Pluripotent Stem Cells via Ecto-Alkaline Phosphatase-Mediated Aggregation of Synthetic Peptides. Cell chemical biology, 24(6), 685–694.e4. https://doi-org.proxy.unibs.it/10.1016/j.chembiol.2017.04.010.

38. González, L. T., Minsky, N. W., Espinosa, L. E., Aranda, R. S., Meseguer, J. P., & Pérez, P. C. (2017). In vitro assessment of hepatoprotective agents against damage induced by acetaminophen and CCl4. BMC complementary and alter-

native medicine, 17(1), 39. https://doi-org.proxy.unibs.it/10.1186/s12906-016-1506-1.

39. Zhang, K., Zhang, L., Liu, W., Ma, X., Cen, J., Sun, Z., Wang, C., Feng, S., Zhang, Z., Yue, L., Sun, L., Zhu, Z., Chen, X., Feng, A., Wu, J., Jiang, Z., Li, P., Cheng, X., Gao, D., Peng, L., … Hui, L. (2018). In Vitro Expansion of Primary Human Hepatocytes with Efficient Liver Repopulation Capacity. Cell stem cell, 23(6), 806–819.e4. https://doi-org.proxy.unibs.it/10.1016/j.stem.2018.10.018.

PUBLISHED MANUSCRIPT

applied sciences

MDPI

Article

Arrangement of Live Human Cells through Acoustic Waves Generated by Piezoelectric Actuators for Tissue Engineering Applications

Marialaura Serzanti [1], Marco Baù [2], Marco Demori [2], Serena Calamaio [1], Manuela Cominelli [3], Pietro Luigi Poliani [3], Patrizia Dell'Era [1,*], Marco Ferrari [2,*] and Vittorio Ferrari [2]

1 Cellular Fate Reprogramming Unit, Department of Molecular and Translational Medicine, University of Brescia, 25121 Brescia, Italy; m.serzanti@unibs.it (M.S.); s.calamaio@unibs.it (S.C.)
2 Department of Information Engineering, University of Brescia, 25121 Brescia, Italy; marco.bau@unibs.it (M.B.); marco.demori@unibs.it (M.D.); vittorio.ferrari@unibs.it (V.F.)
3 Pathology Unit, Department of Molecular and Translational Medicine, University of Brescia, 25121 Brescia, Italy; elemanu2003@libero.it (M.C.); luigi.poliani@unibs.it (P.L.P.)
* Correspondence: patrizia.dellera@unibs.it (P.D.); marco.ferrari@unibs.it (M.F.)

Received: 29 March 2020; Accepted: 14 May 2020; Published: 18 May 2020

Featured Application: The proposed device and method can promote the arrangement of cells in defined geometries through acoustic flexural plate waves for organized engineered tissues.

Abstract: In this paper, the possibility to steer and confine live human cells by means of acoustic waves, such as flexural plate waves (FPWs), generated by piezoelectric actuators applied to non-piezoelectric substrates, has been explored. A device with two lead zirconate titanate (PZT) actuators with an interdigital transducer (IDT) screen-printed on an alumina (Al_2O_3) substrate has been fabricated and tested. The experimental results show that, by exciting the actuators at their resonant frequencies, FPW modes are generated in the substrate. By exploiting the device, arrangements of cells on lines at frequency-dependent distances have been obtained. To maintain the alignment after switching off the actuator, cells were entrapped in a fibrin clot that was cultured for several days, enabling the formation of cellular patterns.

Keywords: acoustic waves; piezoelectric actuators; flexural plate waves (FPWs); in-liquid cell steering and confining; cell manipulation; tissue engineering applications; fibrin gel; myoblasts; endothelial cells

1. Introduction

So-called "tissue engineering science" refers to the practice of combining cells, biomaterials, and suitable biochemical and physicochemical factors to assemble a biological functional tissue. Tissue engineering science is emerging as a promising technique to build functional constructs that restore, maintain, or improve damaged tissues [1].

The physical and structural properties of the tissue, along with biological and biochemical environments, play key roles in achieving cell differentiation, maturation, and organogenesis [2]. Hence, the field of tissue engineering relies on the search for a three-dimensional (3D) scaffold representing a template for tissue formation that can be used in vivo, where it can act as a guidance for cellular regeneration, or can be seeded in vitro with cells and growth factors or subjected to biophysical/mechanical/chemical stimuli that promote tissue growth [3].

A crucial step in building a 3D tissue lies in its thickness, because the exceeding of a certain size (from 100 to 200 μm) prevents the oxygen, nutrients, and metabolic exchange among cell layers, irreparably leading to tissue necrosis [4]. To overcome this issue, current strategies rely on in vitro settings that increase the diffusion/perfusion of the tissue, such as a dynamic culture, while in vivo the colonization of the tissue by host vessels after grafting is promoted. Nevertheless, as happens in natural tissues, the fabrication of a network of microvessels that can be integrated with the host vasculature, could increase the survival of cells more sensitive to reduction of supply of nutrients and oxygen [5].

In recent research activities, 3D bioprinting, wherein both the layer-by-layer precise positioning of biological materials, biochemicals, and living cells, and the spatial control of the placement of functional components has been adopted, allowed for the fabrication of 3D structures exploiting bio-mimicry, autonomous self-assembly, and mini-tissue building blocks [6]. These goals can be pursued with the help of different deposition and shaping techniques, such as inkjet, microextrusion, and laser assisted printing, although these innovative technologies require expensive instrumentation. Bioprinters and bioplotters typically adopt piezoelectric or pneumatic devices for depositing cells, even dispersed into a proper liquid solution [7], and have the benefit of the flexibility of customizable patterning design, but have several drawbacks, such as the relatively large amount of time necessary to correctly achieve the spatial location of cells within the hydrogel, and limitations with respect to the density and viscosity of the liquid solution in which the cells need to be dispersed [8]. The main challenge remains the reproduction of the complex microarchitecture of extracellular matrix components with sufficient resolution, in which multiple cell types interact and exert their biological functions [9].

As an alternative, several strategies for cell trapping have been proposed and exploited in the literature. The most straightforward is hydrodynamic cell trapping, where a (series of) microchannel(s) of sufficiently small size in order to trap cells by suction is fabricated within microsystems [10]. Microbioreactors allowing direct-perfusion of culture medium through tissue-engineered constructs may overcome diffusion limitations associated with static culturing and may provide flow-mediated mechanical stimuli. The hydrodynamic stress imposed on cells within scaffolds is directly dependent on scaffold microstructure and on bioreactor configuration [11].

Microfluidic systems based on acoustic waves generated through the piezoelectric effect have recently received a great deal of attention in biological and medical fields for mixing, sorting, separation, counting, and positioning of particles and cells, mostly relying on the nodes and antinodes generated by standing waves [12]. Surface acoustic wave (SAW), bulk acoustic wave (BAW), and FPW (flexural plate wave) acoustic modes can be generated and detected by piezoelectric actuators driven at suitable frequencies to obtain wavelengths in the order of up to 100 μm [13,14]. The forces generated by the interaction between acoustic waves and fluids can be used to actuate fluids and suspended particles, such as cells, at a small scale with micrometric resolution. Additionally, piezoelectric devices have the inherent advantage of allowing contactless operation between the transducer and the electronics [15].

Custom-built microfluidic perfusion bioreactors with integrated ultrasound standing wave traps have been proposed for cartilage tissue engineering [16]. In such devices, acoustic waves and continuous perfusion of the culture medium at a low-shear flow rate promote scaffold-free generation of 3D agglomerates of human articular chondrocytes and enhance cartilage formation by cells of the agglomerates via improved mechanical stimulation and mass transfer rates. A versatile SAW technique has been proposed to control the distance between two isolated cells, to drive the clustering of single cells in defined geometries, by maintaining them in suspension, and transferring them to their adherent state [17]. The typical configuration of the microfluidic devices used for fluid and particle manipulations exploiting SAWs or FPWs requires piezoelectric substrates with interdigital transducers (IDTs) to realize the actuators [18–22].

In this study, the use of screen-printed piezoelectric films for the generation of the FPWs on alumina substrate was explored to assemble 1D cellular structures. The aim was to demonstrate that arrangements of living human cells can be advantageously obtained by acoustic waves with

actuators on generic non-piezoelectric substrates, thereby including transparent substrates typically adopted for the fabrication of microfluidic devices. This is advantageous compared to similar devices, both those based on FPWs and those based on SAWs, because non-piezoelectric substrates ease the patterning of IDTs in different positions without the need to consider the crystallographic orientations. Thus, by adding one or more pairs of IDTs, in principle it could be possible to obtain 2D-cellular structures. From a biological point of view, the use of the proposed device enables the formation of ordered cellular structures that can be merged into an engineered tissue.

2. Design and Fabrication of the Device

A sketch of the device developed to steer and confine cells dispersed in liquid is shown in Figure 1a. The device exploits two piezoelectric actuators placed diametrically opposed on the bottom of a 25 mm in diameter circular alumina (Al_2O_3) substrate to generate standing acoustic waves, as schematically represented in Figure 1b. The distance between pressure nodes, in which the cells are expected to be confined, corresponds to half the wavelength of the generated acoustic waves.

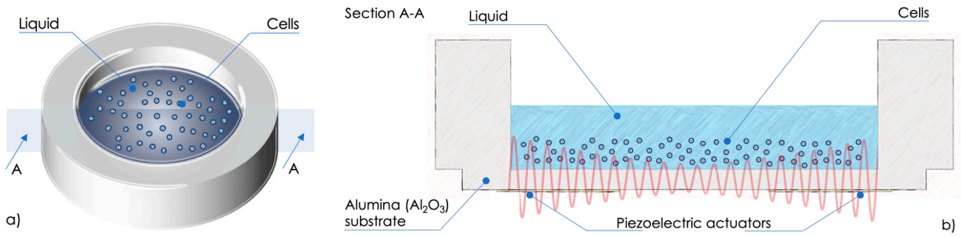

Figure 1. Sketch (**a**) and cross-section A-A (**b**) of the device developed to steer and confine cells dispersed in liquid.

The two piezoelectric actuators have been fabricated by the screen-printing technique [23]. Figure 2a,b show a section and a bottom view of the device, respectively, while Figure 2c shows an enlarged view of a cross-section of the piezoelectric actuator.

The fabrication process of the actuators starts with the screen-printing deposition of a palladium-silver (PdAg) ink to create the bottom 6 mm × 6 mm electrode (connected to pad C) on a 635-µm-thick alumina substrate, as shown in Figure 2d. Then drying at 150 °C and firing at 850 °C processes are applied to finalize the bottom electrode. A lead zirconate titanate (PZT) 8 mm × 8 mm layer is realized on top of the bottom electrode with multiple screen-printing depositions to obtain the final thickness of about 100 µm, as shown in Figure 2e. Drying at 150 °C and firing at 950 °C peak temperature are carried out to each PZT deposition. Finally, an IDT composed of two interleaved comb-shaped arrays of metallic electrodes (connected to pads A and B) is realized on top of the PZT layer by a deposition of PdAg ink, as shown in Figure 2f. Final drying and firing processes are applied to the IDT electrodes, as for the bottom electrode. The IDT has finger width and spacing of 350 µm, as shown in Figure 2c,f.

The PZT layer has been poled at 4 MV/m along the thickness by applying a DC voltage between the two armatures formed by A and B electrically shorted and C, respectively. Thus, a sinusoidal excitation voltage applied between A and B (with C floating), or between A and B electrically shorted and C, generates sinusoidal deformation along the PZT-layer thickness by exploiting mainly the d_{33} mode in both cases, since the thickness of the PZT layer is thinner than the spacing between two adjacent IDT fingers.

Compared to similar devices [12–14], a larger volume of liquid can be used. This is granted by the thickness of the screen-printed PZT film in the order of hundreds of micrometers and typically higher piezoelectric coefficients compared to piezoelectric crystals, thereby providing comparatively higher effectiveness of the actuators. The screen-printed deposition of PZT can be applied to other non-piezoelectric substrates, such as high-temperature glasses, which could grant optical transparency to the device.

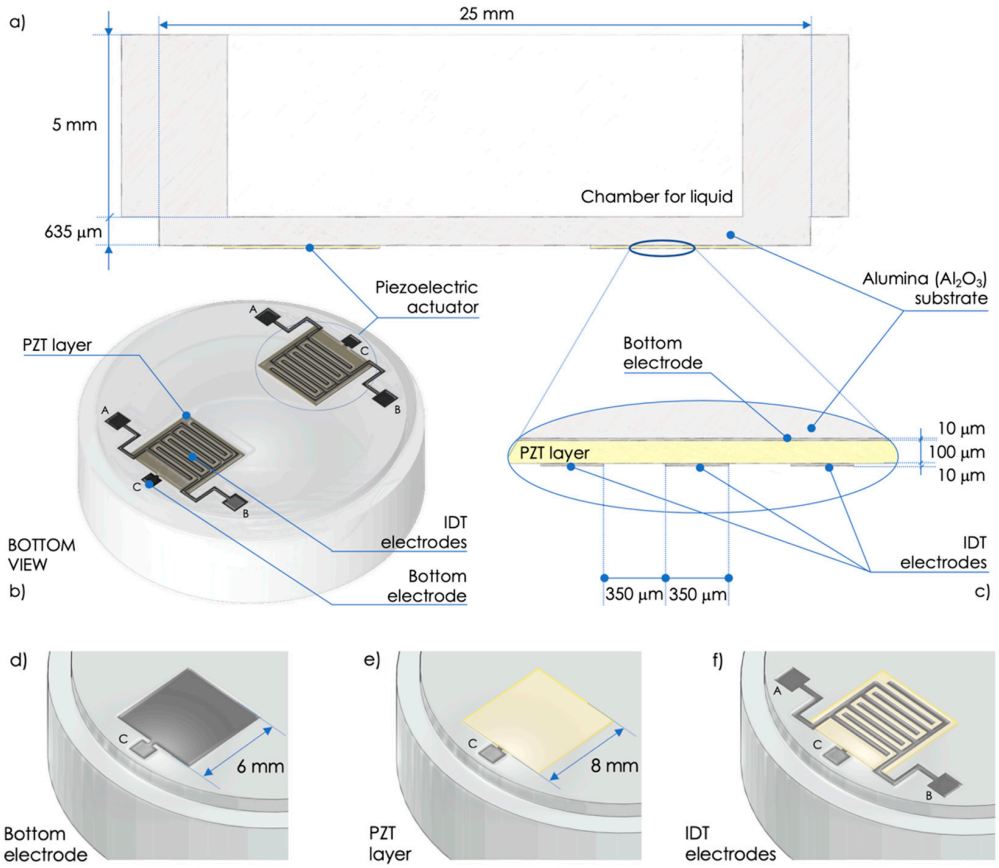

Figure 2. Section (**a**) and bottom view (**b**) of the device. Enlarged view of a cross-section of the piezoelectric actuator (**c**). Fabrication process: deposition of the bottom electrode (**d**), lead zirconate titanate (PZT) layer (**e**), and interdigital transducer (IDT) electrodes (**f**).

Figure 3a,b show top-view and bottom-view pictures of the fabricated device fixed to a printed circuit board (PCB) for electrical connections, respectively. The device can be used by filling the 5-mm-high chamber with liquid in which the cells are dispersed and where the generation of standing acoustic FPWs is expected.

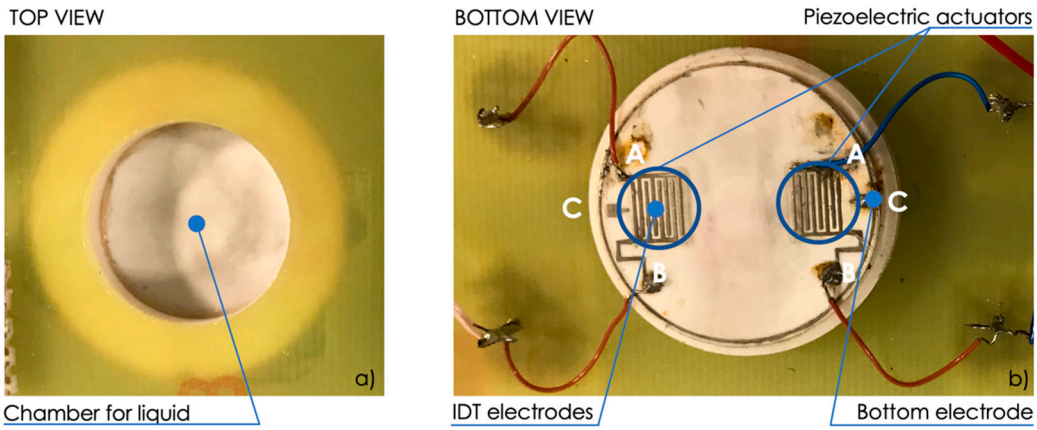

Figure 3. Top-view (**a**) and bottom-view (**b**) pictures of the fabricated device fixed to a printed circuit board (PCB).

3. Materials and Methods

3.1. Reagents

Bovine fibrinogen 90% clottable and bovine thrombin, high purity grade, were purchased from MP Biomedicals. Neutral Red was purchased from AMRESCO. 4',6-Diamidine-2'-phenylindole dihydrochloride (DAPI) was purchased by Sigma.

3.2. Cell Culture

L6 rat myoblasts and human foreskin fibroblasts (HFF; provided by American Type Culture Collection, catalogue #CRL-2429) were maintained in Dulbecco's modified Eagle's medium (Life Technologies) supplemented with 15% (*v*/*v*) fetal bovine serum (Life Technologies), 1% (*v*/*v*) non-essential amino acids (Life Technologies), and 1% (*v*/*v*) penicillin/streptomycin (Life Technologies). Cells were trypsinized every 3 or 4 days and split 1:4, with medium changes every other day.

Human umbilical vein endothelial cells (HUVECs) were isolated from human umbilical cords, used at early (I–IV) passages, and grown on plastic surface coated with 0.1% (*w*/*v*) porcine gelatin in Clonetics® EGM™-2 medium (Lonza). Cells were trypsinized every 3 or 4 days and split 1:4, with medium changes every other day. HUVECs were obtained from pregnant women, in accordance with the protocol approved by the Ethics Committee of Brescia (protocol number 1842).

Human adipose-derived mesenchymal stem cells (hMSCs) were obtained from a previous study described in [24]. Cells were maintained in Iscove's modified Dulbecco's medium containing 5% (*v*/*v*) human platelet lysate (STEMCELL™ Technologies) and 2U/mL heparin (Sigma). Cells were trypsinized every 3 or 4 days, and subcultures were seeded at 5000 cells/cm^2 with medium changes every other day. Cells from a single donor were used up to passage 6.

For human samples, written informed consents were obtained from patients in accordance with the Declaration of Helsinki.

3.3. Cell Viability Tests

Cells were counted using TC20™ Automated Cell Counter (BIO-RAD) that exploits auto-focus technology and sophisticated cell counting algorithms to produce accurate cell counts in less than 30 s. Viability tests were performed by adding to cell suspension one volume of the Trypan Blue Dye, 0.4% (*w*/*v*) solution. The presence of the blue dye inside a cell leads the machine to consider it as dead cells, thereby enabling the calculation of cell viability. Results are then reported as a percentage of total cell number.

3.4. Cell Staining

For the Neutral Red staining, cells were detached, resuspended in phosphate buffer saline (PBS) containing 40 µg/mL Neutral Red, incubated for 20 min, and directly used for the experiment.

For the nuclear fluorescent staining, DAPI was diluted to a final concentration of 1 µg/mL and incubated for 5 min. Cells were then washed twice with PBS before imaging.

3.5. Cell Alignment

Cells were detached and counted. A total of 10^6 cells were resuspended in 0.5 mL ice-cold culture medium. Cell suspension was transferred to the chamber for the actuation and the following microscopical observation.

To embed the cells in a clot, 10 mg/mL fibrinogen was added to cell culture medium without serum. Just before the transfer to the chamber for actuation, 2 µL of thrombin solution (200 U/mL in 0.9% NaCl) was added to the cell suspension. Actuation was performed for 5 min at the indicated frequency in order to allow for a complete clot polymerization.

The clot was transferred to a cell culture multiwell plate, covered with cell medium, and observed in the following days.

3.6. Clot Histology and Antibody Staining

Fibrin clot was fixed in 4% (*w*/*v*) paraformaldehyde (Bio-Optica) and processed for inclusion. The 2-µm-thick representative sections from paraffin embedded blocks were de-waxed and rehydrated. Endogenous peroxidase activity was blocked with 0.3% (*v*/*v*) H_2O_2 (Sigma Aldrich) in methanol for 20 min. Antigen retrieval was performed using a microwave oven in 1.0 mM EDTA (Carlo Erba) buffer (pH 8.0).

Sections were then washed in tris-buffered saline (TBS, Carlo Erba) (pH 7.4) and incubated for one hour in the specific primary antibody diluted in TBS 1% (*w*/*v*) bovine serum albumin (BSA) (CD31 (clone PECAM-1) Novocastra TM 1:50).

The signal was revealed using the DAKO Envision+System-HRP Labelled Polymer Anti-Mouse, followed by diaminobenzydine (DAB) as chromogen and hematoxylin as counterstain.

4. Results and Discussion

4.1. Electrical Characterization of the Device

The IDT actuators have been characterized experimentally in order to extract the frequencies at which the maximum FPW generation effectiveness is expected. Figure 4a,b show the admittances $Y_{A\text{-}B}$ and $Y_{AB\text{-}C}$ measured between A and B while C was floating, and between A and B electrically shorted and C, respectively.

The resonant frequencies of the two configurations, i.e., the frequencies where the conductance reaches a maximum [25,26], are at about 6.7 and 8.0 MHz for $Y_{A\text{-}B}$, and at about 6.0 and 7.2 MHz for $Y_{AB\text{-}C}$. These frequencies are expected to correspond to the propagation of FPW modes in the substrate [27,28].

A tailored electronic interface has been developed to drive the actuators. Figure 5 shows a block diagram of the interface. The excitation signals were generated by a programmable direct digital synthesizer (DDS, AD9959) that allowed us to excite the actuators with two independent channels and provided the possibility of setting both the common excitation frequency and the phase difference between the channels.

Dedicated power amplifiers (ADA4870) have been adopted as the output stage to properly drive the actuators. The electronic interface excites the actuators with a sinusoidal signal with peak-to-peak amplitude and frequency of up to 20 V and 15 MHz, respectively.

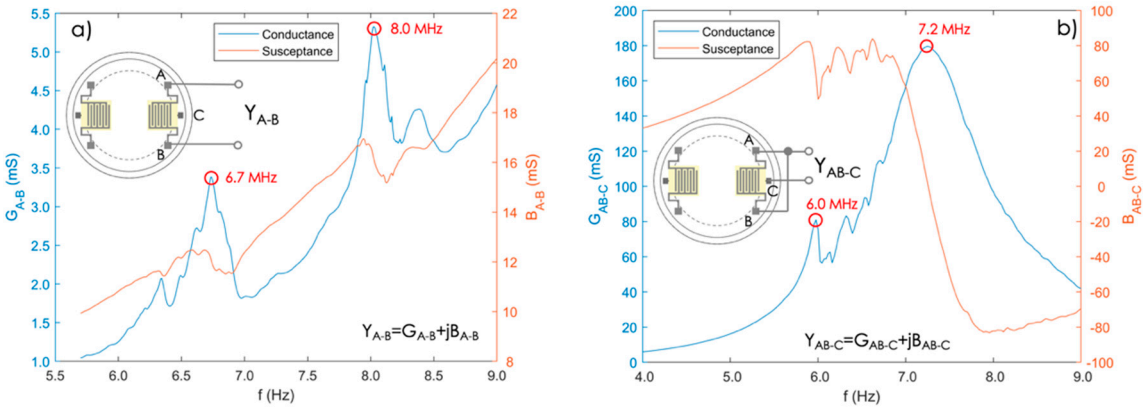

Figure 4. Measured admittance $Y_{A\text{-}B}$ (**a**) and $Y_{AB\text{-}C}$ (**b**) as functions of frequency. The plots show resonances at frequencies around 6.7 and 8.0 MHz (**a**) and around 6.0 and 7.2 MHz (**b**).

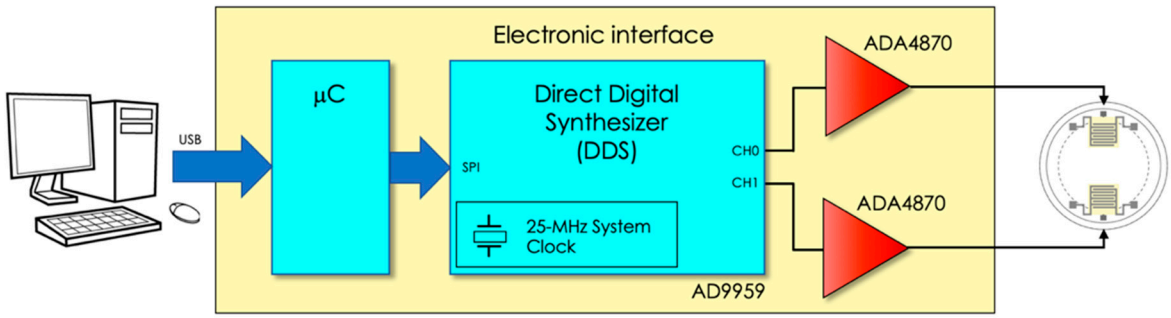

Figure 5. Block diagram of the tailored electronic interface used to drive the actuators.

4.2. Alignment of Cells

Preliminary tests have been carried out to verify the capability of the device to generate acoustic waves that lead to alignment of a cellular suspension. Cells to be aligned were detached from the culture dish, dispersed in PBS as single cells, stained with the live dye Neutral Red, and put in the chamber of the device. Figure 6 shows the experimental setup with the device placed under the optical microscope and the tailored electronic interface used to drive the piezoelectric actuators.

Initially, different concentrations of cells were tested in order to identify the amount required to appreciate the alignment in the volume of 500 µL, starting from 2×10^5 cells/mL and reaching 4×10^6 cells/mL. From these experiments, 2×10^6 cells/mL was identified as the optimal concentration for the formation of distinct lines of single cells, and therefore this amount was used for all the following experiments.

Since the survival of L6 rat myoblasts despite acoustic wave exposition was critical, this cell line was used to verify that the actuation was not hampering cell viability. The experiment was set up by exposing different samples with the same cell concentrations to FPWs for different lengths of time. Cell viability was then measured by trypan blue cell exclusion (Table 1). Since cell viability remained high even at long times, a 5-min actuation period was chosen for all the following experiments.

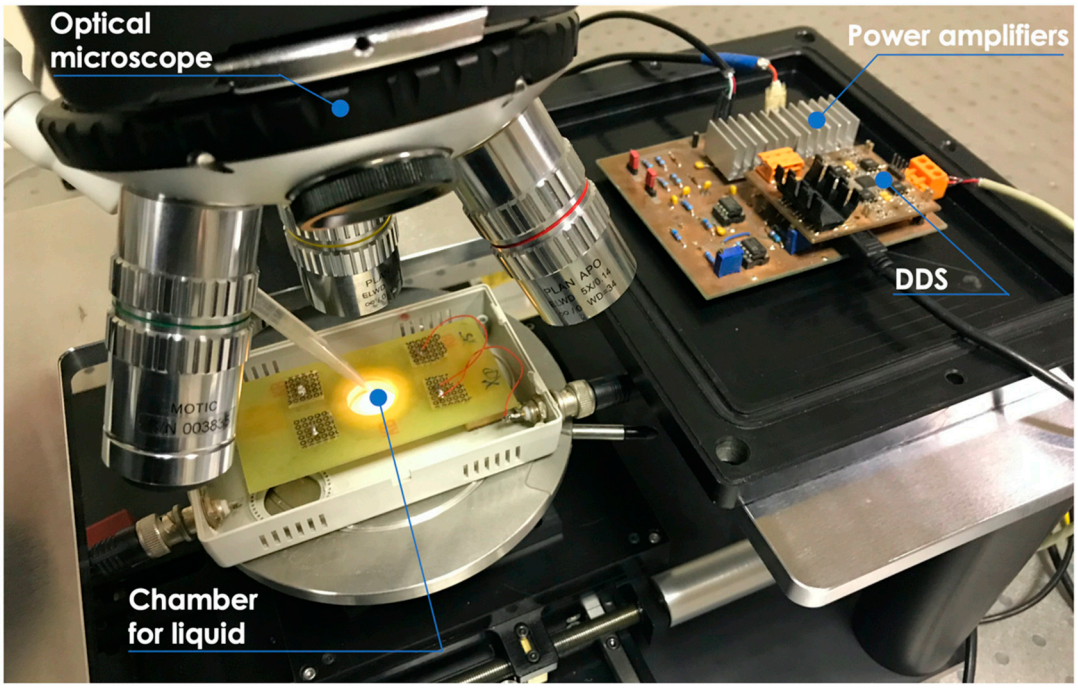

Figure 6. Experimental setup with the device placed under the optical microscope and the tailored electronic interface used to drive the piezoelectric actuators.

Table 1. Cell viability as a function of the actuation time of the device.

Actuation Time (min)	Cell Viability (%)
2	100
4	98
5	100
7	98

Different wavelengths were tested to verify the effects on the alignment of human fibroblasts (HFF) by exciting a single actuator with a sinusoidal signal applied to A and B (C was floating). To demonstrate the alignment of cells induced by the acoustic waves, HFF dispersed in PBS were used, since their viability is unaffected by the acoustic field.

The distance d between the different pressure nodes in the fluid, in which the cells are expected to be confined, corresponds to half the wavelength of the acoustic waves, resulting $d = \lambda/2 = v/2f_e$, where v = 1500 m/s is the expected propagation velocity of the acoustic waves into PBS, and f_e is the excitation frequency. Figure 7a,b show the results obtained with f_{e1} = 6.7 MHz and f_{e2} = 8.0 MHz, for which distances $d_1 = v/2f_{e1}$ = 112 µm and $d_2 = v/2f_{e2}$ = 93.8 µm are expected, respectively.

As it can be observed, an increase of the excitation frequency, i.e., decrease of the wavelength, corresponds to a decrease in the distance between lines. The mean distances between the cell alignments $d_{1,mean}$ = 121 µm and $d_{2,mean}$ = 103 µm, which are in good agreement with predictions, have been estimated from the gray-scale intensity plots derived from the insets. Similar results have been obtained by exciting a single actuator with a sinusoidal signal applied to A and B (shorted) and C with frequencies of 6.0 and 7.2 MHz (not shown).

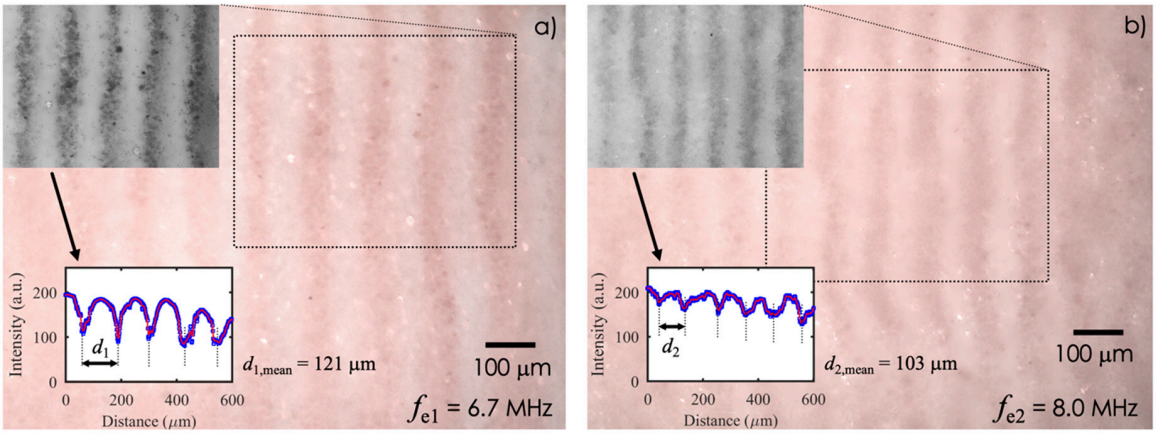

Figure 7. Effects of different wavelengths of acoustic waves on a human foreskin fibroblast (HFF) cell suspension. Cell accumulation in lines caused by the acoustic waves generated by exciting a single IDT at f_{e1} = 6.7 MHz (**a**) and f_{e2} = 8.0 MHz (**b**), respectively. The mean distances $d_{1,mean}$ = 121 µm and $d_{2,mean}$ = 103 µm have been estimated from the gray-scale intensity plots derived from the insets.

4.3. Entrapment of Cells in a Matrix

Switching off the actuator lets the cells scatter in the fluid, thereby losing the alignment. Hence, to maintain the cell alignment and separation, actuated cells have been entrapped in a 3D matrix.

To allow for wave propagation, a low-viscosity fluid capable of going through a sol–gel transition in a short time was needed, in which the polymerization had to start after the alignment. During the time needed for the sol–gel transition of the culture medium, i.e., five min in our experiments, the cell viability could be affected, given the impossibility of the cells, during this time, to make contact through the integrins with proteins of the cell matrix, a mechanism that has already been showed to regulate cell viability [29]. Relying on previous experience in the angiogenesis field, a fibrin gel, obtained by adding thrombin to a liquid fibrinogen solution, was used, rather than other biomaterials,

such as inert substrates mixed or linked to extracellular matrix molecules [8,30]. Besides, the survival of fibroblasts [31,32], fibroblasts/myoblasts [33], and HUVECs [34,35] in the fibrin gel has already been widely demonstrated. Cells were subsequently resuspended in a 10 mg/mL fibrinogen solution maintained at 4 °C, and thrombin 0.4 U was added just before transferring the cell suspension into the chamber. After five minutes, the fibrin clot was formed and aligned cells were entrapped in the matrix. For a long-term culture, the clots containing the cells were transferred to a cell culture dish, covered with cell culture medium, and observed in the following days. A 6.7 MHz excitation frequency was chosen for the following experiments.

The first experiments were done using rat myoblasts that, although totally alive after the actuation process, did not survive the following 24 hour culture, thereby suggesting that the stiffness of the fibrin matrix may not represent the correct environment for myoblast survival [36].

The next set of experiments was therefore performed with HFF. These cells entrapped in the fibrin clot maintained the aligned geometry for several days, as evidenced in Figure 8a–c, respectively. Of note, the magnification box in Figure 8a shows that each line is composed of single cells. Starting from 48 h, cells showed cytoplasmic protrusions, reflecting cell health, that became more complex over time, as shown in Figure 8d by a histological section of the clot and by the higher magnification box.

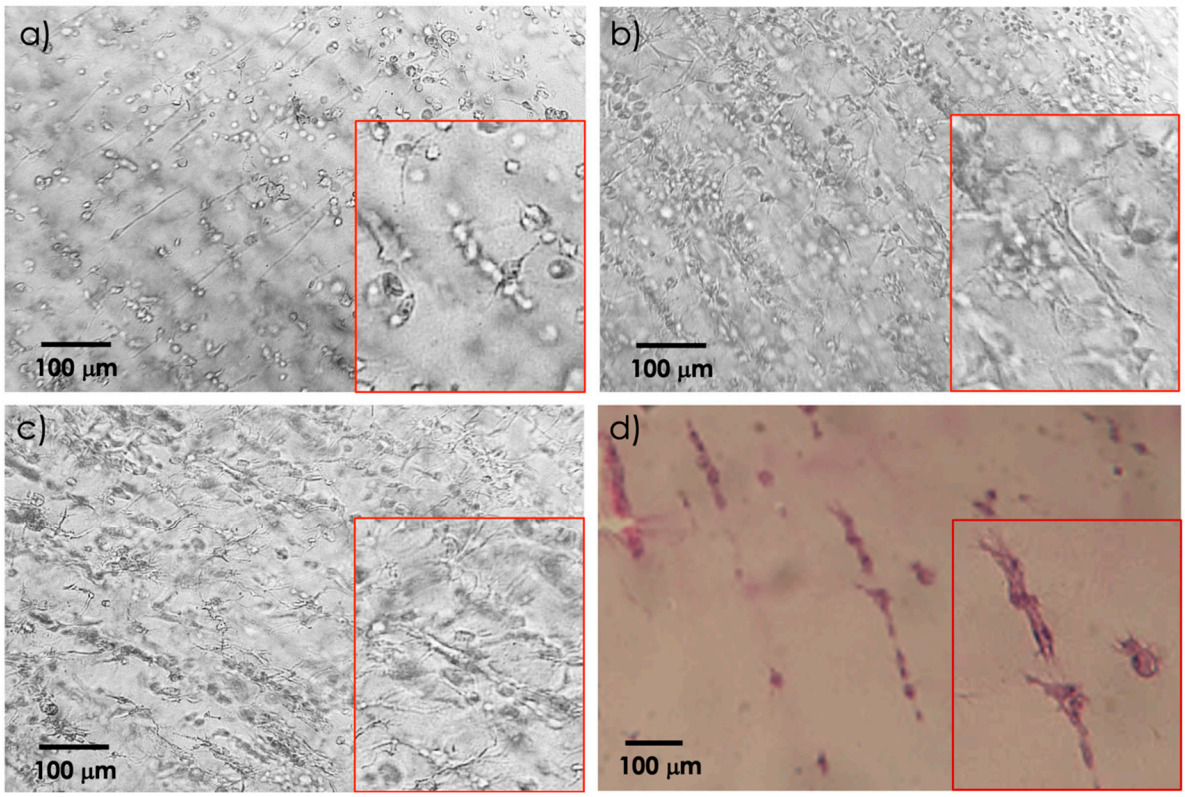

Figure 8. Aligned HFF in fibrin clot maintained in culture for 24 (**a**), 48 (**b**), and 72 h (**c**) with higher magnification boxes. Histological section of (hematoxylin and eosin)-stained cells at 72 h (**d**) with a higher magnification box.

4.4. Entrapment of Endothelial Cells in the Fibrin Clot

Angiogenesis assays are normally based on the capacity of endothelial cells to invade gels of different origins, mainly collagen or fibrin, and to form capillary-like structures [37]. Since the alignment could represent a preliminary step for the formation of a capillary, human endothelial cells were challenged in the device to verify the hypothesis that the process can promote it. Indeed, aligned HUVECs tend to form structures that become more complex during time. At 96 h

these structures still comprise several cells, as shown by microscope observations and nuclear DAPI staining in Figure 9a,b, respectively.

Next, the clot containing these structures was fixed, embedded in paraffin, and sliced, and the various sections underwent an immunochemical reaction with antibodies recognizing the CD31 endothelial antigen. In these conditions, HUVECs maintain the aligned organization that comprises a hole, as shown in Figure 9c.

To confirm that the alignment was based on a mechanical process, rather than a biological interaction, HUVECs were mixed with MSCs before the actuation. As those cells had similar sizes, their distribution along the pressure nodes was not clustered by cell type, as shown in Figure 9d. The presence of MSCs does not alter the cellular alignment, but the release of trophic factors characteristics of this type of cell [26,38] inhibits the formation of the hole, and promotes the formation of several cytoplasmic protrusions of HUVECs that are still recognized by their CD31 expression.

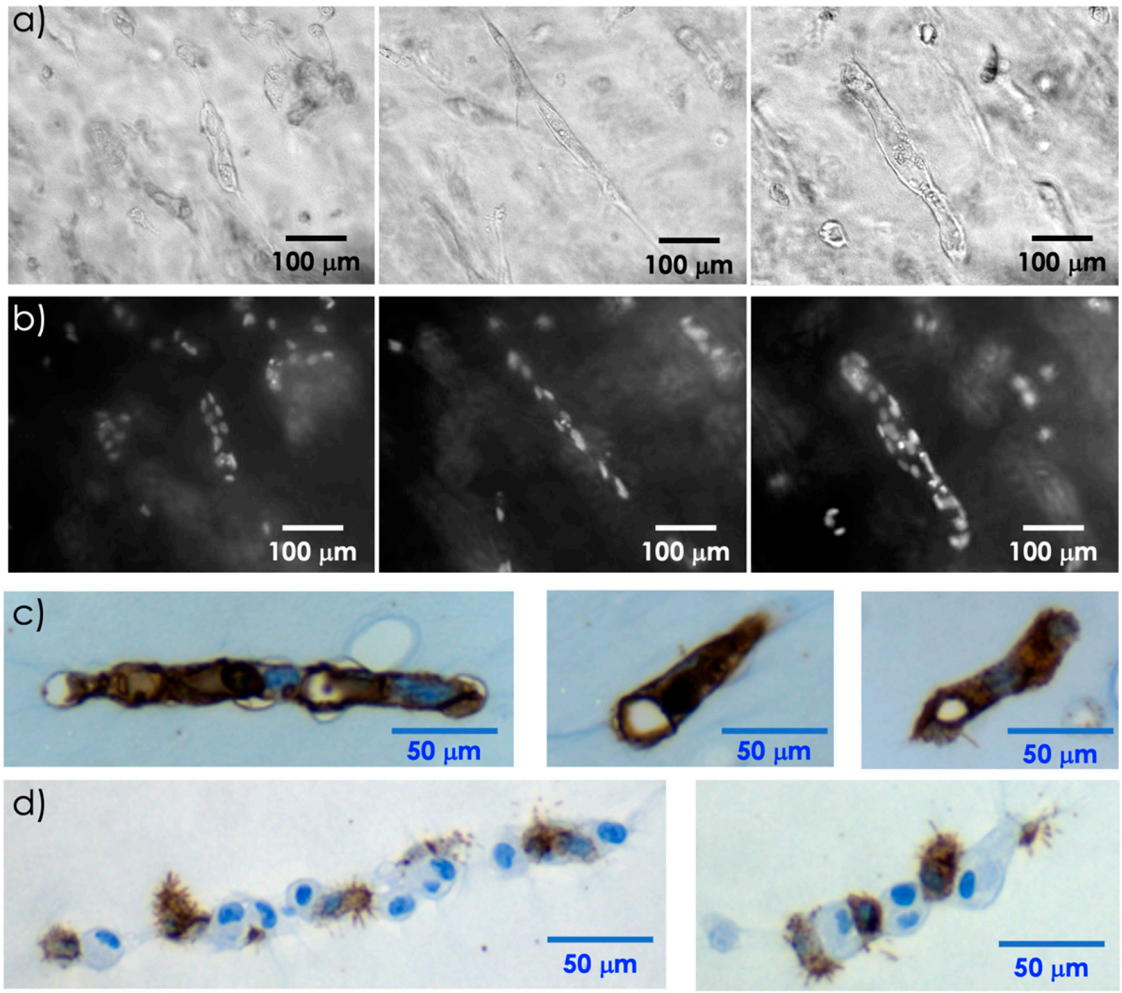

Figure 9. Aligned endothelial cells in fibrin clot at 96 h (**a**). DAPI staining showing cellular nuclei (**b**). CD31 (clone PECAM-1) staining of clot-entrapped human umbilical vein endothelial cells (HUVECs) (**c**). CD31 staining of clot-entrapped HUVECs and hMSCs (**d**).

5. Conclusions

The use of PZT actuators to generate acoustic waves in non-piezoelectric substrates has been proposed to steer and confine cells dispersed in liquid. A test device with two screen-printed PZT actuators used to generate acoustic waves on alumina substrate has been fabricated. The proposed device has the advantage of exploiting an inexpensive substrate which does not need to be piezoelectric, thereby allowing to use of high-temperature reinforced glasses which have the property of being

transparent. A tailored electronic circuit has been developed to generate the excitation signals for the actuators. Experimental results demonstrate that, by exciting a single actuator at its resonant frequencies, FPW modes are generated in the substrate. Accumulation of cells dispersed in liquid on lines can be obtained by selecting the proper excitation frequency. These results confirm the capability of the proposed PZT actuators to generate acoustic waves for applications in microfluidic devices as controlled positioning of cells dispersed in liquid.

From a biological point of view, devices similar to the one proposed are required to obtain ordered structures for tissue engineering purposes. Indeed, alignment of cells is a key step in several biological processes. For example, the basic unit of a muscle, i.e., the fiber, is formed by the fusion of several myocytes whose aligned actin and myosin molecules will produce effective muscle contraction [39]. Moreover, in engineered tissues, the presence of blood vessels that allow the distribution of nutrients or the cellular waste removal is an essential requirement. Therefore, the effective realization of an engineered tissue cannot be disjointed from an adequate architecture that, as shown, can be obtained using acoustic waves.

Author Contributions: Design and development of the device, M.F., M.D., M.B., and V.F.; experimental activity, M.B., M.D., M.S., S.C., and M.C.; analysis of experimental data, M.F., P.L.P., and P.D.; writing—original draft preparation, M.F. and P.D.; drawings, M.F.; writing—review and editing, M.F., M.B., V.F., M.S., and S.C.; funding acquisition, M.F, V.F., and P.D. All authors have read and agreed to the published version of the manuscript.

Funding: This research was funded by the project "MIcrosystems MeRging ACoustics and fLuidics to build human engineered tissuE (MIRACLE)" funded by University of Brescia in the context of "Health and Wealth 2015" athenaeum grant and partially supported by Fondazione Cariplo (grant number 2014-0822).

Conflicts of Interest: The authors declare no conflict of interest.

References

1. Guilak, F.; Butler, D.L.; Goldstein, S.A.; Baaijens, F.P. Biomechanics and mechanobiology in functional tissue engineering. *J. Biomech.* **2014**, *47*, 1933–1940. [CrossRef] [PubMed]
2. Bajaj, P.; Schweller, R.M.; Khademhosseini, A.; West, J.L.; Bashir, R. 3D biofabrication strategies for tissue engineering and regenerative medicine. *Annu. Rev. Biomed. Eng.* **2014**, *16*, 247–276. [CrossRef] [PubMed]
3. O'Brein, F.J. Biomaterials & scaffolds for tissue engineering. *Mater. Today* **2011**, *14*, 88–95.
4. Ratcliffe, A.; Niklason, L.E. Bioreactors and bioprocessing for tissue engineering. *Ann. N. Y. Acad. Sci.* **2002**, *961*, 210–215. [CrossRef] [PubMed]
5. Neumann, T.; Nicholson, B.S.; Sanders, J.E. Tissue engineering of perfused microvessels. *Microvasc. Res.* **2003**, *66*, 59–67. [CrossRef]
6. Murphy, S.V.; Atala, A. 3D bioprinting of tissues and organs. *Nat. Biotechnol.* **2014**, *32*, 773–785. [CrossRef]
7. The, R.; Yamaguchi, S.; Ueno, A.; Akiyama, Y.; Morishima, K.; Yamaguchi, S.; Ueno, A.; Akiyama, Y. Piezoelectric inkjet-based one cell per one droplet automatic printing by image processing. In Proceedings of the 2013 IEEE/RSJ International Conference on Intelligent Robots and Systems, Tokyo, Japan, 3–7 November 2013; pp. 502–507.
8. Naseer, S.M.; Manbachi, A.; Samandari, M.; Walch, P.D.K.; Gao, Y.; Zhang, Y.S.; Davoudi, F.; Wang, W.; Abrinia, K.; Cooper, J.M.; et al. Surface acoustic waves induced micropatterning of cells in gelatin methacryloyl (GelMA) hydrogels. *Biofabrication* **2017**, *9*, 015020. [CrossRef]
9. Song, K.; Wang, Z.; Liu, R.; Chen, G.; Liu, L. Microfabrication-Based Three-Dimensional (3-D) Extracellular Matrix Microenvironments for Cancer and Other Diseases. *Int. J. Mol. Sci.* **2018**, *19*, 935. [CrossRef]
10. Perry, J.L.; Kandlikar, S.G. Review of fabrication of nanochannels for single phase liquid flow. *Microfluid. Nanofluidics* **2006**, *2*, 185–193. [CrossRef]
11. Raimondi, M.; Moretti, M.; Cioffi, M.; Giordano, C.; Boschetti, F.; Laganà, K.; Pietrabissa, R. The effect of hydrodynamic shear on 3D engineered chondrocyte systems subject to direct perfusion. *Biorheol.* **2006**, *43*, 215–222.
12. Luo, J.K.; Fu, Y.Q.; Milne, W.I. Acoustic Wave Based Microfluidics and Lab-on-a-Chip. In *Modeling and Measurement Methods for Acoustic Waves and for Acoustic Microdevices*; IntechOpen: London, UK, 2013; pp. 515–556. [CrossRef]

13. Bouyer, C.; Chen, P.; Güven, S.; Demirtaş, T.T.; Nieland, T.J.F.; Padilla, F.; Demirci, U. A Bio-Acoustic Levitational (BAL) Assembly Method for Engineering of Multilayered, 3D Brain-Like Constructs, Using Human Embryonic Stem Cell Derived Neuro-Progenitors. *Adv. Mater.* **2016**, *28*, 161–167. [CrossRef] [PubMed]
14. Chen, Y.; Ding, X.; Lin, S.-C.S.; Yang, S.; Huang, P.-H.; Nama, N.; Zhao, Y.; Nawaz, A.A.; Guo, F.; Wang, W.; et al. Tunable Nanowire Patterning Using Standing Surface Acoustic Waves. *ACS Nano* **2013**, *7*, 3306–3314. [CrossRef] [PubMed]
15. Demori, M.; Baù, M.; Ferrari, M.; Ferrari, V. Interrogation Techniques and Interface Circuits for Coil-Coupled Passive Sensors. *Micromachines* **2018**, *9*, 449. [CrossRef] [PubMed]
16. Li, S.; Glynne-Jones, P.; Andriotis, O.G.; Ching, K.Y.; Jonnalagadda, U.S.; Oreffo, R.; Hill, M.; Tare, R.S. Application of an acoustofluidic perfusion bioreactor for cartilage tissue engineering. *Lab Chip* **2014**, *14*, 4475–4485. [CrossRef]
17. Guo, F.; Li, P.; French, J.B.; Mao, Z.; Zhao, H.; Li, S.; Nama, N.; Fick, J.R.; Benkovic, S.J.; Huang, T.J. Controlling cell–cell interactions using surface acoustic waves. *Proc. Natl. Acad. Sci. USA* **2015**, *112*, 43–48. [CrossRef]
18. Shilton, R.; Tan, M.K.; Yeo, L.Y.; Friend, J. Particle concentration and mixing in microdrops driven by focused surface acoustic waves. *J. Appl. Phys.* **2008**, *104*, 14910. [CrossRef]
19. Ding, X.; Lin, S.-C.S.; Kiraly, B.; Yue, H.; Li, S.; Chiang, I.-K.; Shi, J.; Benkovic, S.J.; Huang, T.J. On-chip manipulation of single microparticles, cells, and organisms using surface acoustic waves. *Proc. Natl. Acad. Sci. USA* **2012**, *109*, 11105–11109. [CrossRef]
20. Orloff, N.D.; Dennis, J.R.; Cecchini, M.; Schonbrun, E.; Rocas, E.; Wang, Y.; Novotný, D.; Simmonds, R.W.; Moreland, J.; Takeuchi, I.; et al. Manipulating particle trajectories with phase-control in surface acoustic wave microfluidics. *Biomicrofluidics* **2011**, *5*, 044107. [CrossRef]
21. Ai, Y.; Sanders, C.K.; Marrone, B.L. Separation of Escherichia coli Bacteria from Peripheral Blood Mononuclear Cells Using Standing Surface Acoustic Waves. *Anal. Chem.* **2013**, *85*, 9126–9134. [CrossRef]
22. Guo, F.; Mao, Z.; Chen, Y.; Xie, Z.; Lata, J.P.; Li, P.; Ren, L.; Liu, J.; Yang, J.; Dao, M.; et al. Three-dimensional manipulation of single cells using surface acoustic waves. *Proc. Natl. Acad. Sci. USA* **2016**, *113*, 1522–1527. [CrossRef]
23. Baù, M.; Ferrari, M.; Tonoli, E.; Ferrari, V. Sensors and energy harvesters based on piezoelectric thick films. *Procedia Eng.* **2011**, *25*, 737–744. [CrossRef]
24. De Luca, A.; Verardi, R.; Neva, A.; Benzoni, P.; Crescini, E.; Xia, E.; Almici, C.; Calza, S.; Dell'Era, P. Comparative Analysis of Mesenchymal Stromal Cells Biological Properties. *ISRN Stem Cells* **2013**, *2013*, 1–9. [CrossRef]
25. Ferrari, M.; Ferrari, V.; Marioli, D. Interface circuit for multiple-harmonic analysis on quartz resonator sensors to investigate on liquid solution microdroplets. *Sens. Actuators B Chem.* **2010**, *146*, 489–494. [CrossRef]
26. Arnau, A.; García, J.V.; Jiménez, Y.; Ferrari, V.; Ferrari, M. Improved electronic interfaces for AT-cut quartz crystal microbalance sensors under variable damping and parallel capacitance conditions. *Rev. Sci. Instrum.* **2008**, *79*, 75110. [CrossRef]
27. Demori, M.; Baù, M.; Ferrari, M.; Ferrari, V. Particle Manipulation by Means of Piezoelectric Actuators for Microfluidic Applications. *Lect. Notes Electr. Eng.* **2017**, *457*, 223–228. [CrossRef]
28. Demori, M.; Baù, M.; Dalola, S.; Ferrari, M.; Ferrari, V. Piezoelectric Actuators for In-Liquid Particle Manipulation in Microfluidic Applications. *Proceeding* **2017**, *1*, 392. [CrossRef]
29. Schwartz, M.; Assoian, R.K. Integrins and cell proliferation: Regulation of cyclin-dependent kinases via cytoplasmic signaling pathways. *J. Cell Sci.* **2001**, *114*, 2553–2560.
30. Sanzari, I.; Humphrey, E.J.; Dinelli, F.; Terracciano, C.M.; Prodromakis, T. Effect of patterned polyacrylamide hydrogel on morphology and orientation of cultured NRVMs. *Sci. Rep.* **2018**, *8*, 11991. [CrossRef]
31. Balestrini, J.L.; Billiar, K.L. Equibiaxial cyclic stretch stimulates fibroblasts to rapidly remodel fibrin. *J. Biomech.* **2006**, *39*, 2983–2990. [CrossRef]
32. Paye, M.; Nusgens, B.; Lapière, C. Factor XIII of Blood Coagulation Modulates Collagen Biosynthesis by Fibroblasts in vitro. *Pathophysiol. Haemost. Thromb.* **1989**, *19*, 274–283. [CrossRef]
33. Li, M.; Dickinson, C.E.; Finkelstein, E.B.; Neville, C.; Sundback, C.A. The Role of Fibroblasts in Self-Assembled Skeletal Muscle. *Tissue Eng. Part A* **2011**, *17*, 2641–2650. [CrossRef] [PubMed]

34. Nakatsu, M.; Sainson, R.C.; Aoto, J.N.; Taylor, K.L.; Aitkenhead, M.; Pérez-Del-Pulgar, S.; Carpenter, P.M.; Hughes, C.C. Angiogenic sprouting and capillary lumen formation modeled by human umbilical vein endothelial cells (HUVEC) in fibrin gels: The role of fibroblasts and Angiopoietin-1☆. *Microvasc. Res.* **2003**, *66*, 102–112. [CrossRef]
35. Nakatsu, M.; Hughes, C.C. Chapter 4 An Optimized Three-Dimensional In Vitro Model for the Analysis of Angiogenesis. *Methods Enzymol.* **2008**, *443*, 65–82. [CrossRef] [PubMed]
36. Gérard, C.; Forest, M.A.; Beauregard, G.; Skuk, D.; Tremblay, J.P. Fibrin Gel Improves the Survival of Transplanted Myoblasts. *Cell Transplant.* **2012**, *21*, 127–138. [CrossRef]
37. Taraboletti, G.; Giavazzi, R. Modelling approaches for angiogenesis. *Eur. J. Cancer* **2004**, *40*, 881–889. [CrossRef]
38. Hofer, H.R.; Tuan, R.S. Secreted trophic factors of mesenchymal stem cells support neurovascular and musculoskeletal therapies. *Stem Cell Res. Ther.* **2016**, *7*, 131. [CrossRef]
39. Lieber, R.L. Skeletal muscle adaptability. I: Review of basic properties. *Dev. Med. Child Neurol.* **1986**, *28*, 390–397. [CrossRef]